Electronic Supplementary Material (ESI) for Polymer Chemistry.

ELECTRONIC SUPPORTING INFORMATION

Versatile Functionalization of Polymer Nanoparticles with Carbonate Groups via Hydroxyurethane Linkages

Neha Yadav, Farzad Seidi, Silvano Del Gobbo, Valerio D´Elia,* Daniel Crespy*

Department of Materials Science and Engineering, School of Molecular Science and Engineering, Vidyasirimedhi Institute of Science and Technology (VISTEC), Rayong 21210, Thailand

Table S1. Synthesis of P(GCMA-*co*-MMA) copolymers by miniemulsion copolymerization of GCMA and MMA at 70 ˚C for 16 h.

Entry	Polymer	Monomer [mol%]		Solid Content [%]	Diameter	
		GCMA	MMA		D_h [nm]	PDI
1	P(GCMA)	100 (100)[a]	0 (0)[a]	63	134	0.21
2	P(GCMA-*co*-MMA)	50 (63.75)[a]	50 (36.25)[a]	95	116	0.19
3	P($GCMA_{0.91}$-*co*-$MMA_{0.9}$)[b]	75 (84.47)[a]	25 (16.63)[a]	72	139	0.20

[a] Amount of monomer in mg

[b] Composition determined by ^{1}H NMR spectroscopy in DMSO-d6.

Table S2. Elemental analysis of polymer nanoparticles after reaction with various amines, dialysis, and drying.

Material	Amine/5CCs [mol%]	C [%]	N [%]	H [%]	N/C (% molar ratio)
P-BA 1	50	54.3	1.3	6.2	2.0
P-BA 3	200	59.7	4.0	6.6	5.9
P-HMDA 2	100	52.4	2.6	7.2	4.2
P-Arg 2	200	54.1	1.4	6.8	2.2
P-Lys 2	200	53.0	1.3	6.2	2.1
P-Alb 1	50[a]	52.3	3.5	6.1	5.9
P-Alb 3	200[a]	52.0	3.2	6.1	5.3
P-Dop	200[a]	55.3	4.5	6.6	7.1

[a] wt% ratio of albumin to P(GCM-*co*-MMA) nanoparticles.

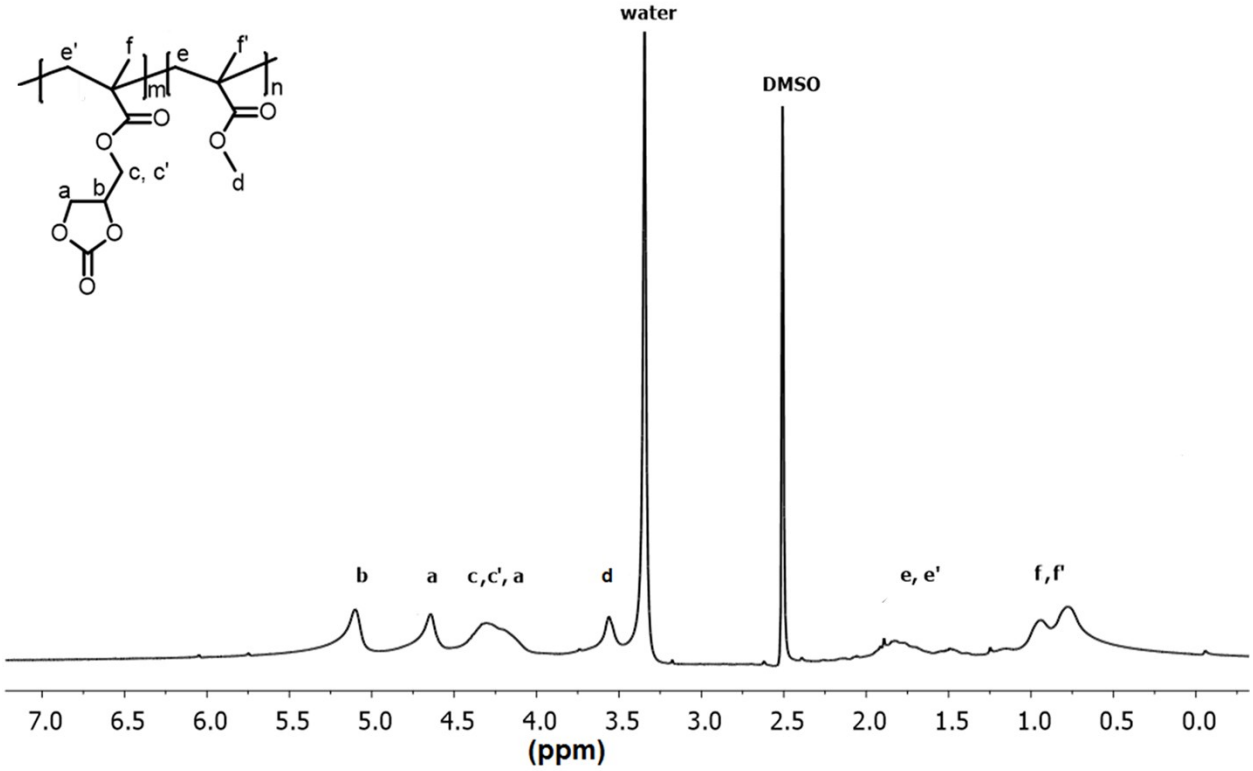

Figure S1. ^{1}H-NMR spectrum of P(GCMA-co-MMA) dissolved in DMSO-d_6 synthesized by miniemulsion polymerization after purification and drying.

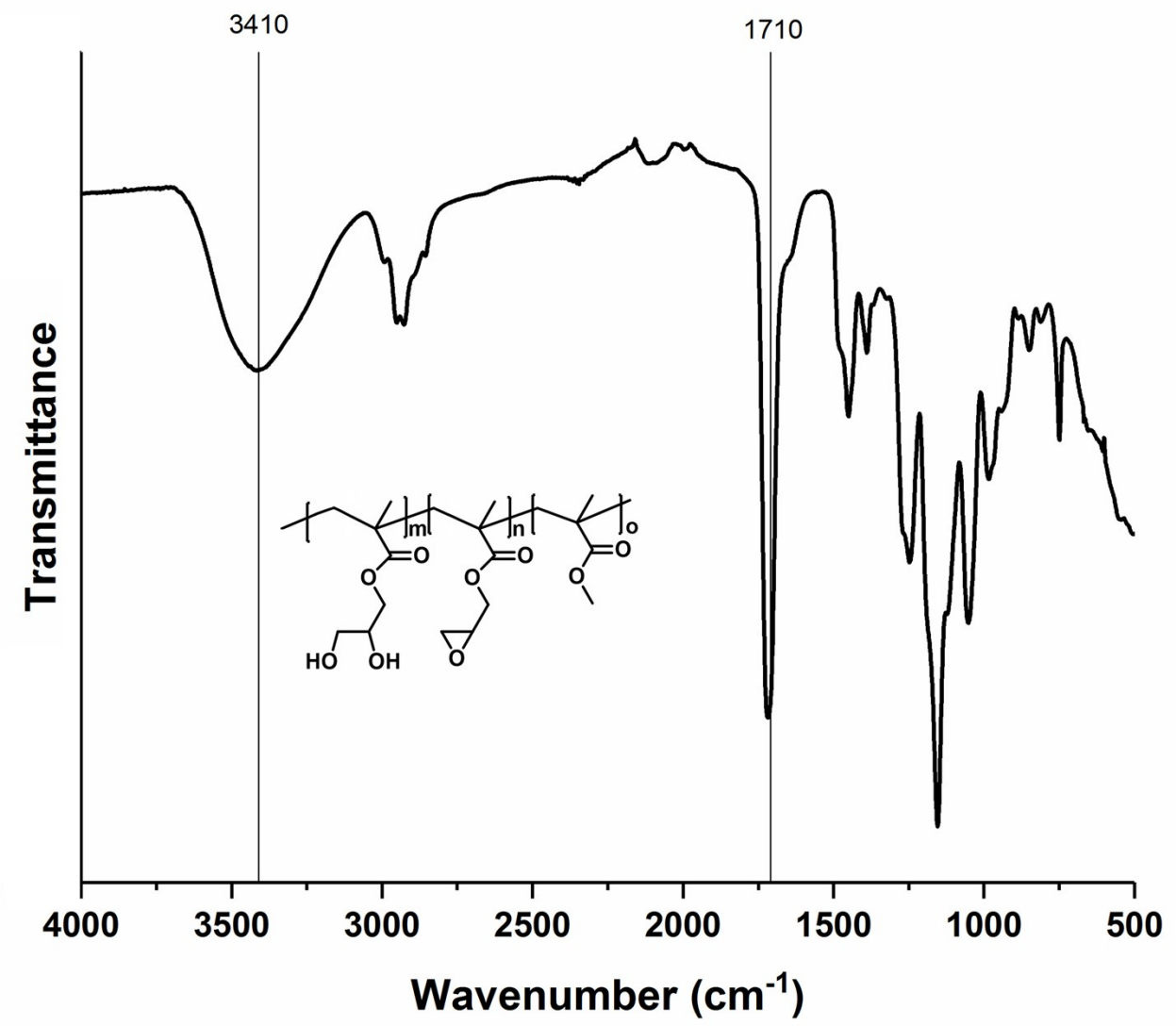

Figure S2. IR spectra of hydrolyzed copolymer of glycidyl methacrylate (GMA) with methyl methacrylate (MMA) obtained by miniemulsion copolymerization at 70 ˚C for 24 h.

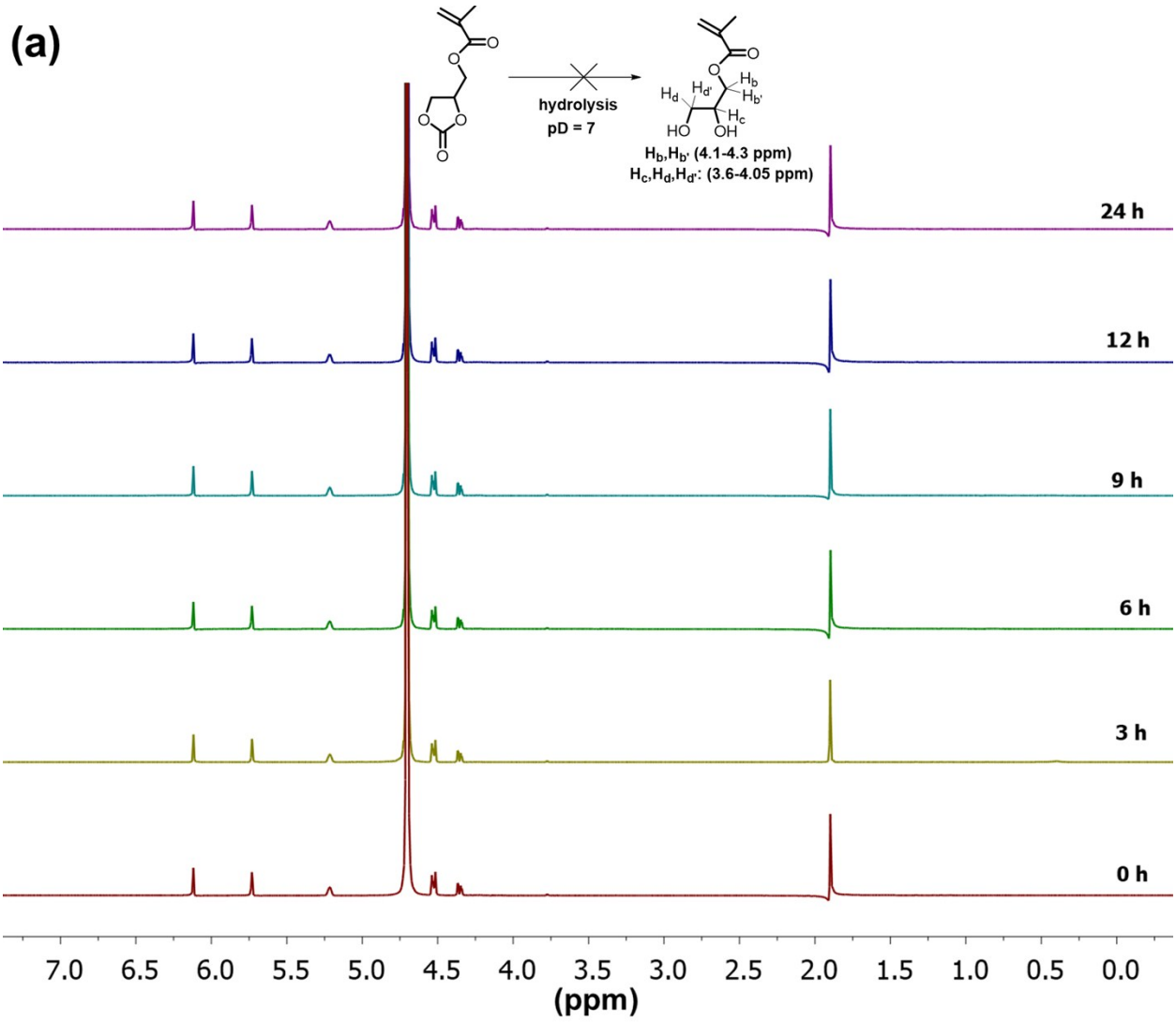
(a)
hydrolysis
pD = 7
Hb,Hb' (4.1-4.3 ppm)
Hc,Hd,Hd': (3.6-4.05 ppm)
24 h
12 h
9 h
6 h
3 h
0 h
7.0 6.5 6.0 5.5 5.0 4.5 4.0 3.5 3.0 2.5 2.0 1.5 1.0 0.5 0.0
(ppm)

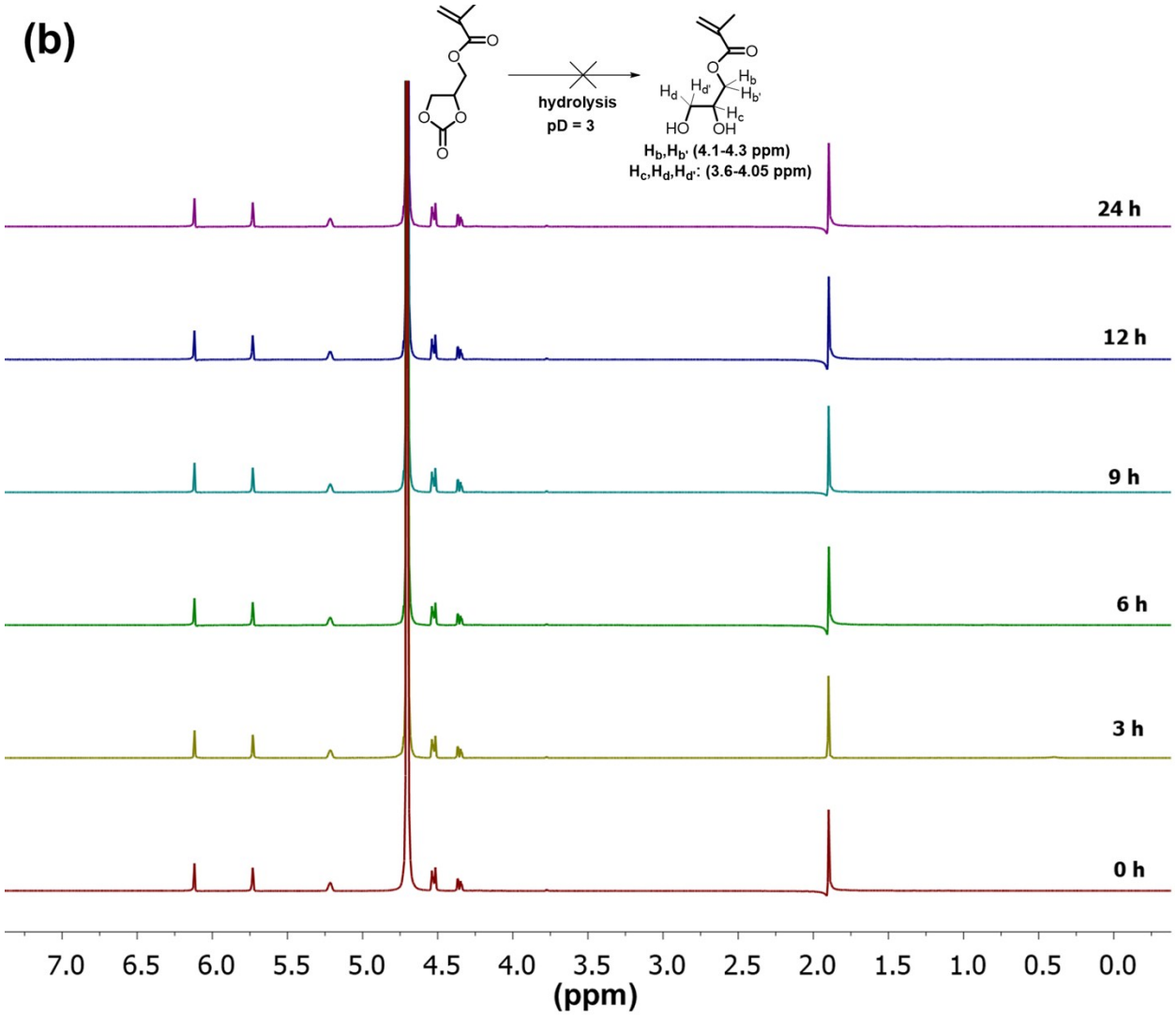
(b)
hydrolysis
pD = 3
H_b,$H_{b'}$ (4.1-4.3 ppm)
H_c,H_d,$H_{d'}$: (3.6-4.05 ppm)
24 h
12 h
9 h
6 h
3 h
0 h
7.0 6.5 6.0 5.5 5.0 4.5 4.0 3.5 3.0 2.5 2.0 1.5 1.0 0.5 0.0
(ppm)

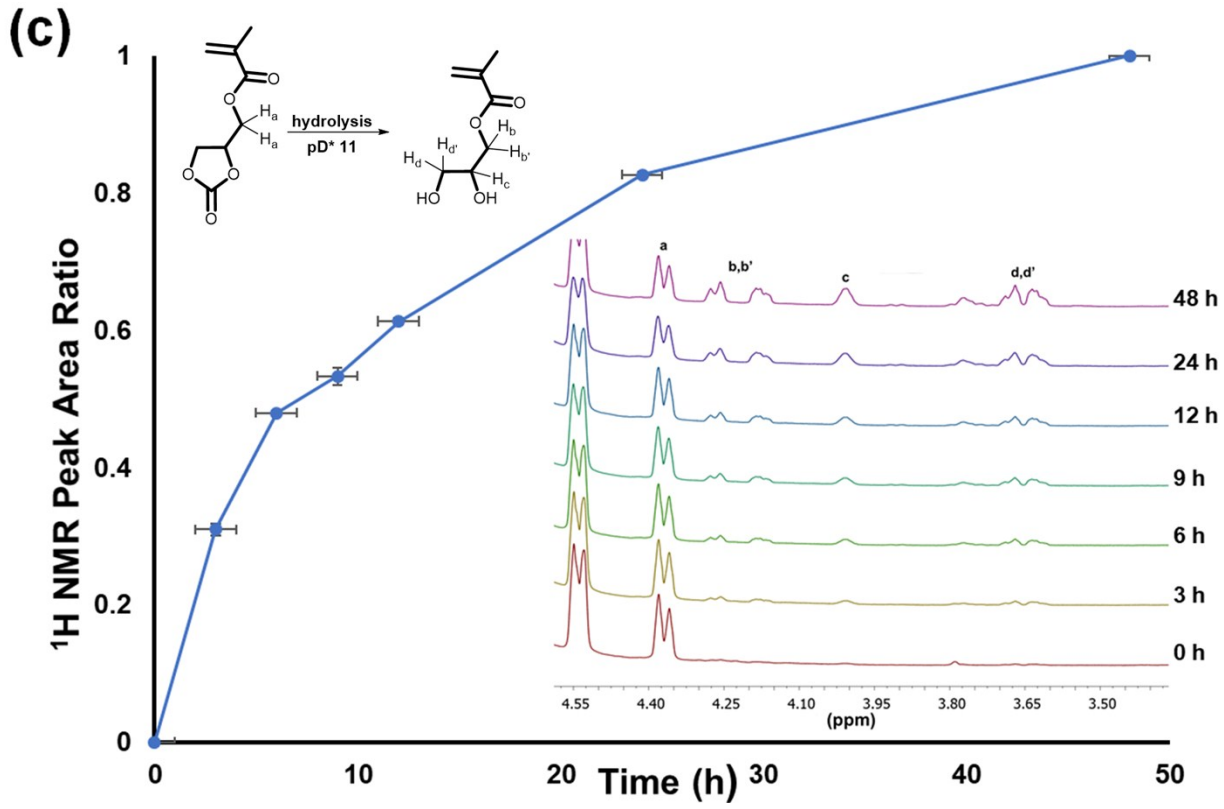

Figure S3. ^{1}H-NMR spectra of GCMA in D_2O at pD 7 (a), pD 3 (b), and pD 11 (c) Hydrolysis kinetics of GCMA at pD 11 expressed as ratio of NMR signals integrals ($I_{b+b'}/I_a$).

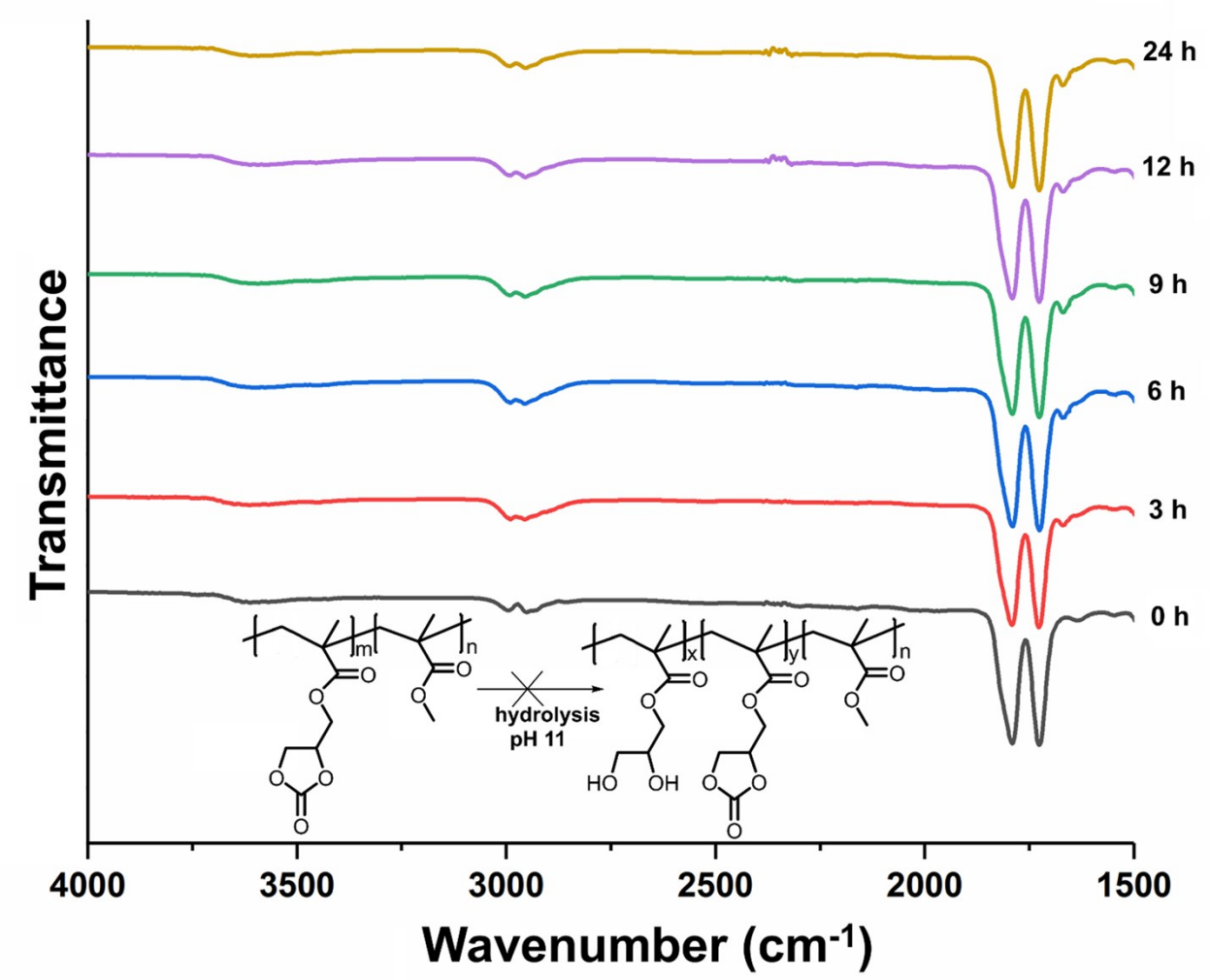

Figure S4. IR spectra of P(GCMA-*co*-MMA) at various time intervals in D_2O after purification and drying of nanoparticles dispersed in a buffer solution at pH 11.

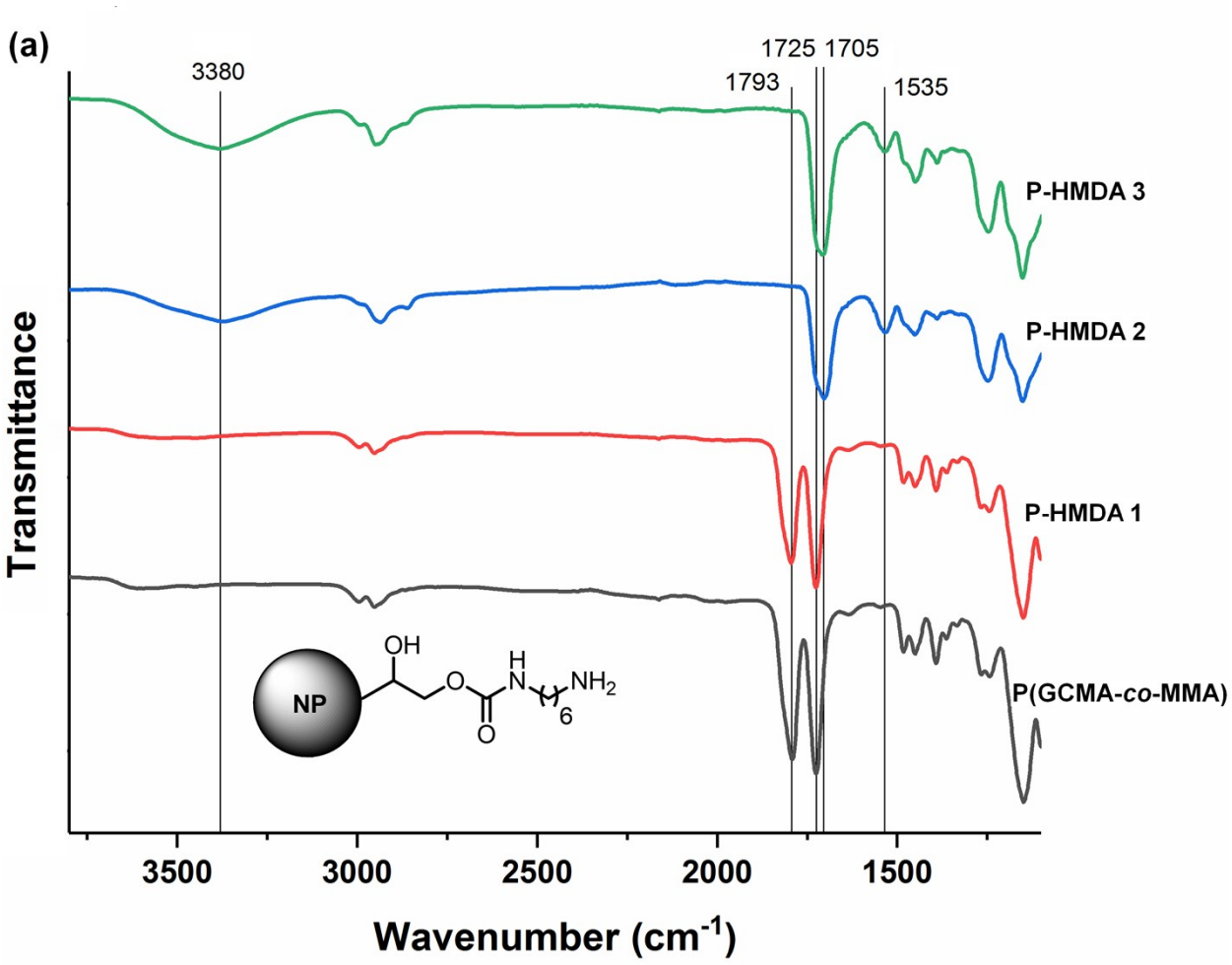
(a)
3380
1793
1725
1705
1535
P-HMDA 3
P-HMDA 2
P-HMDA 1
P(GCMA-co-MMA)
Transmittance
NP
OH
O
H
N
NH2
6
O
3500
3000
2500
2000
1500
Wavenumber (cm-1)

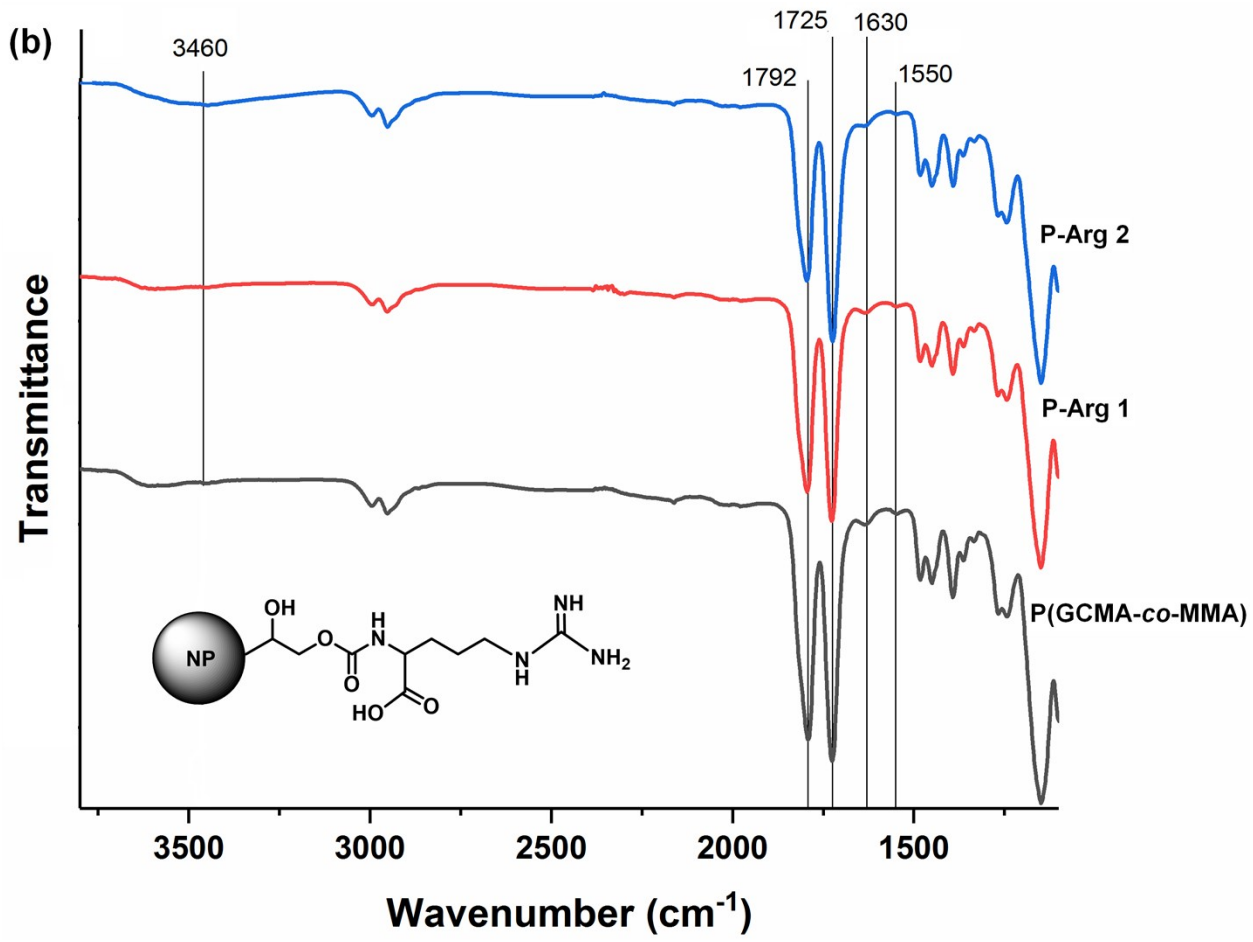
(b)
3460
1792
1725
1630
1550
P-Arg 2
P-Arg 1
P(GCMA-co-MMA)
Transmittance
NP
OH
O
H
N
O
HO
O
NH
N
H
NH2
3500
3000
2500
2000
1500
Wavenumber (cm-1)

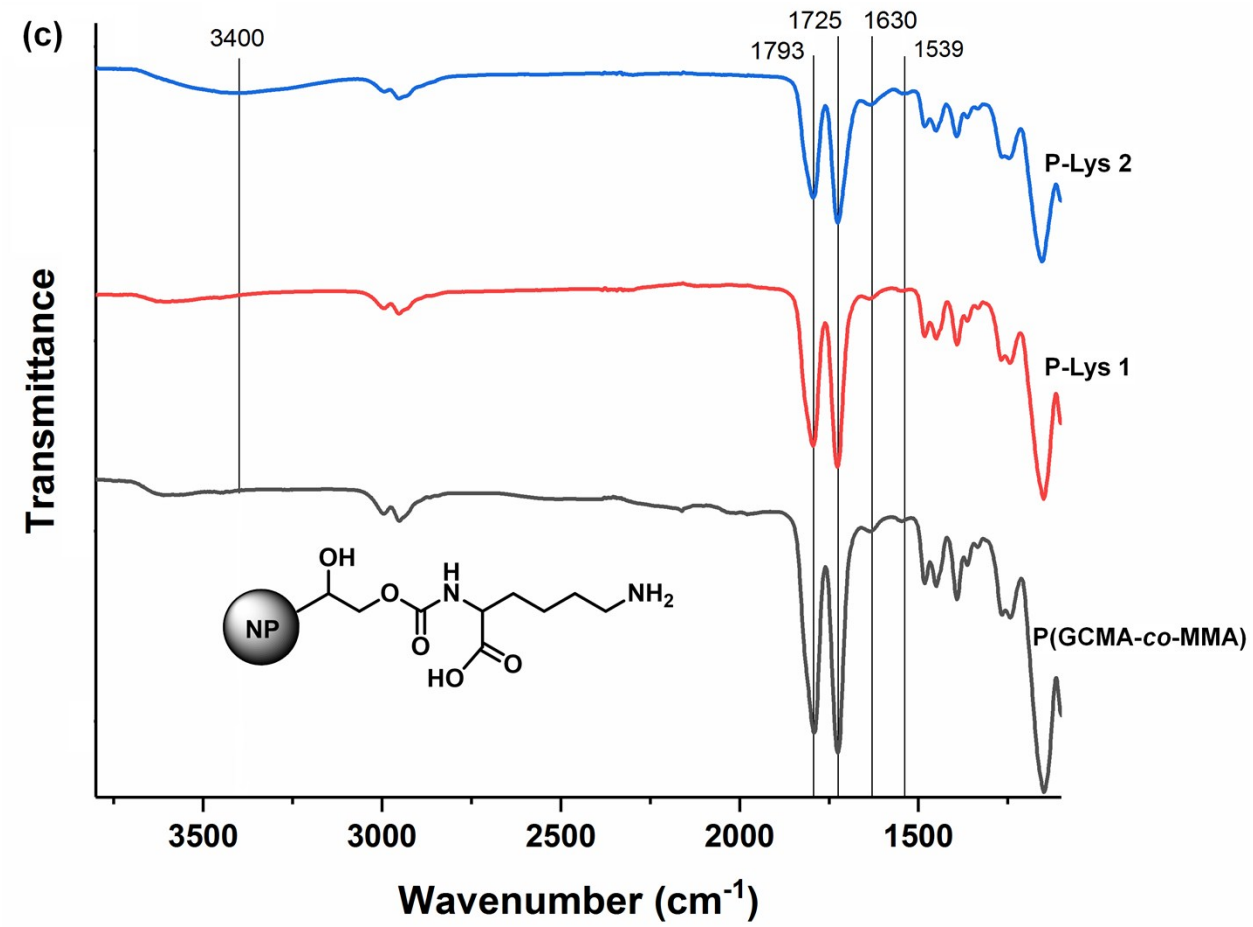
(c)
3400
1793
1725
1630
1539
P-Lys 2
P-Lys 1
P(GCMA-co-MMA)
Transmittance
NP
OH
O
H
N
NH2
O
HO
O
3500
3000
2500
2000
1500
Wavenumber (cm-1)

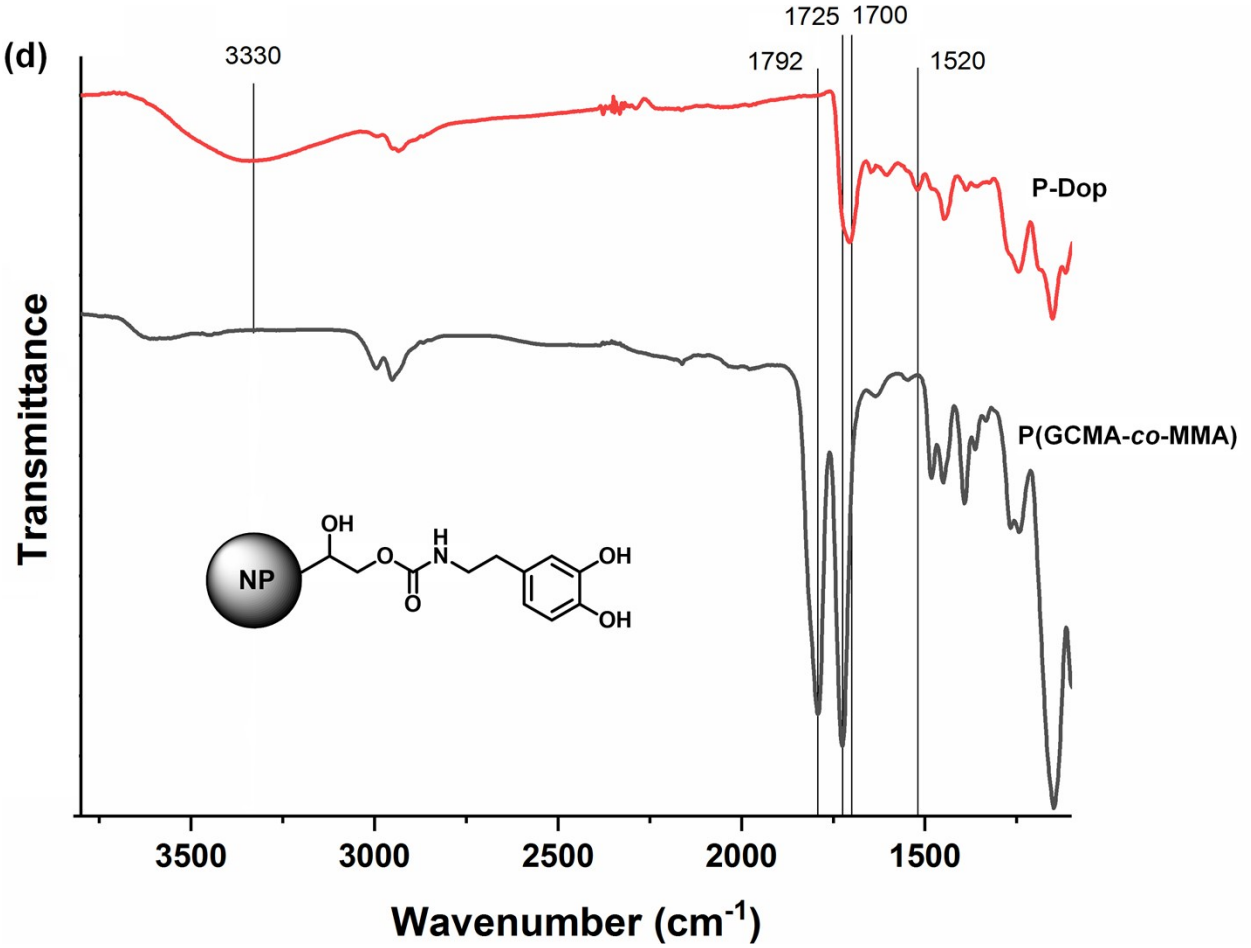

Figure S5. IR spectra of purified and dried polymers before and after functionalization of P(GCMA-*co*-MMA) nanoparticles with HMDA (a), arginine (b), L-lysine (c), dopamine (d).

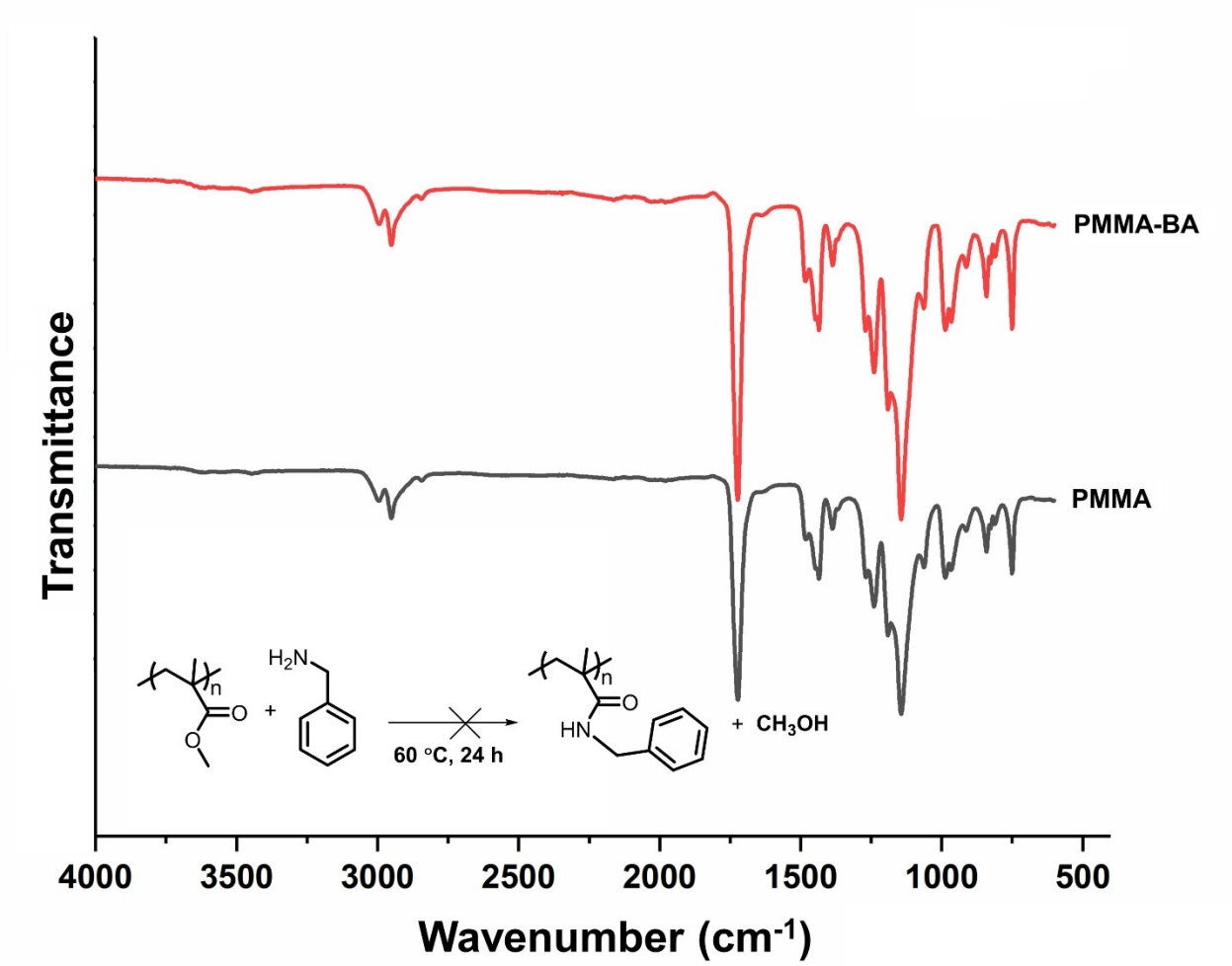

Figure S6. IR spectra of PMMA before and after dissolution in DMSO in the presence of benzyl amine.

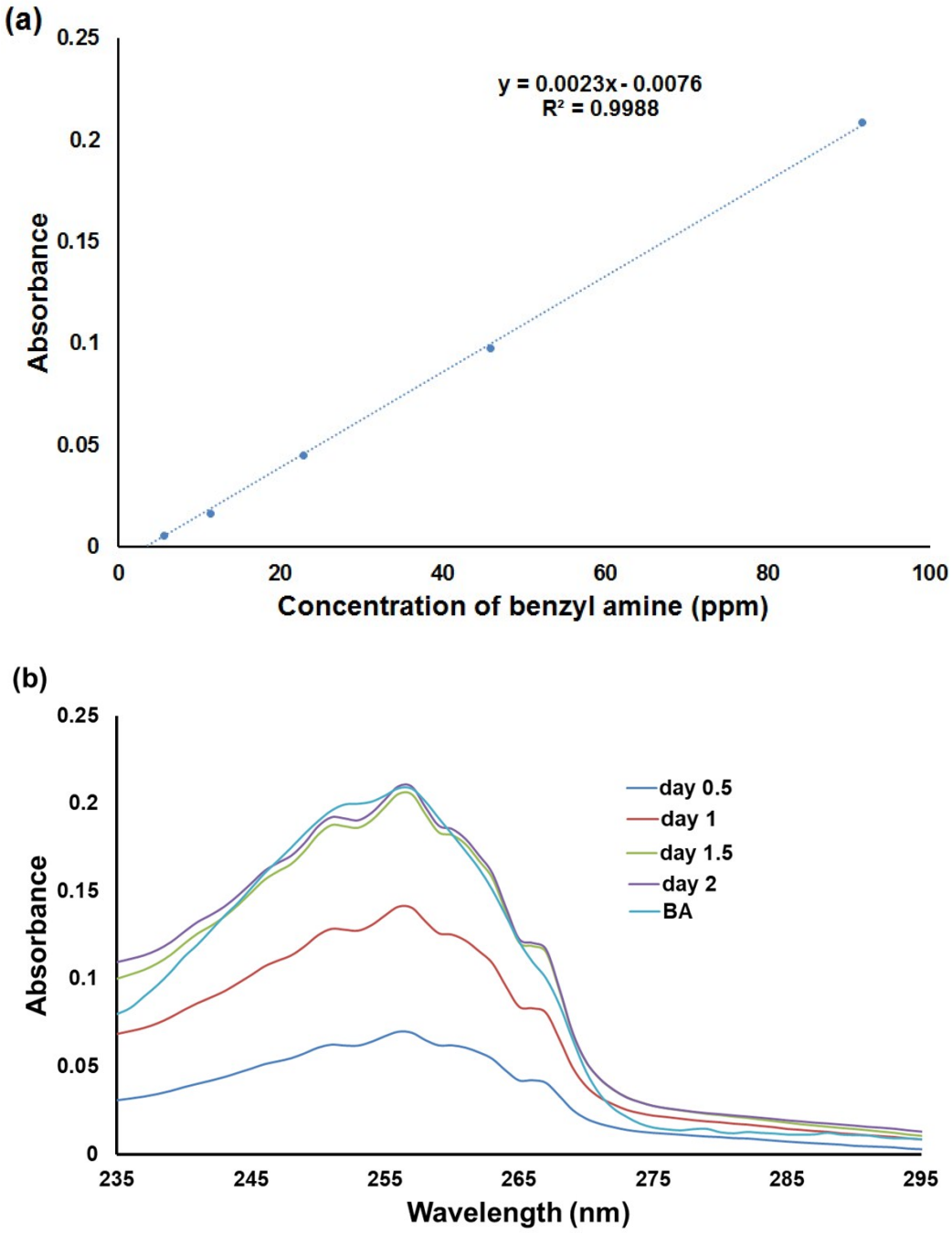

Figure S7. (a) Calibration curve for determining the concentration of benzylamine based on absorbance at 257 nm; (b) UV absorbance spectra of dialysis media of P-BA 3 dispersion (diluted 130 times in water).

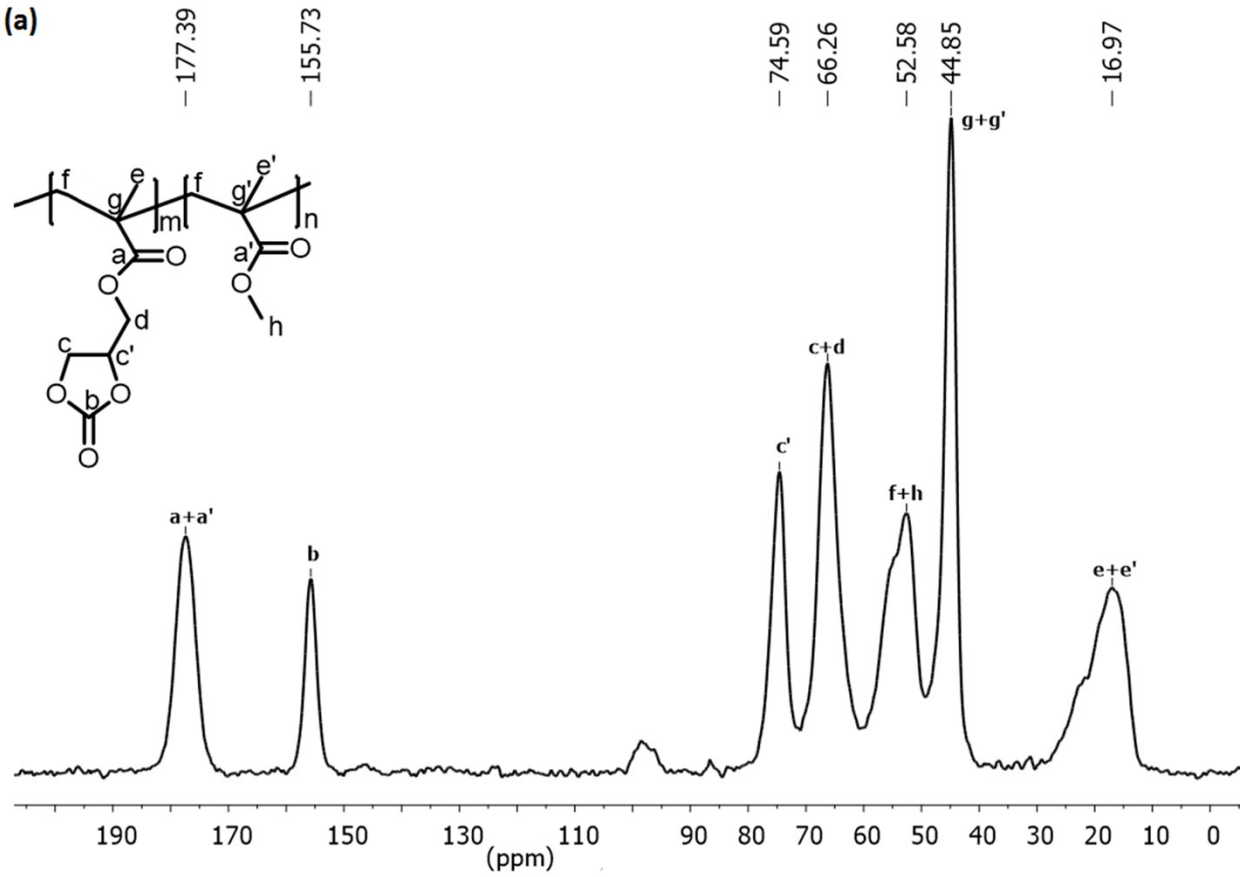
(a)
177.39
155.73
74.59
66.26
52.58
44.85
16.97
g+g'
c+d
c'
f+h
a+a'
b
e+e'
190
170
150
130
110
90
80
70
60
50
40
30
20
10
0
(ppm)

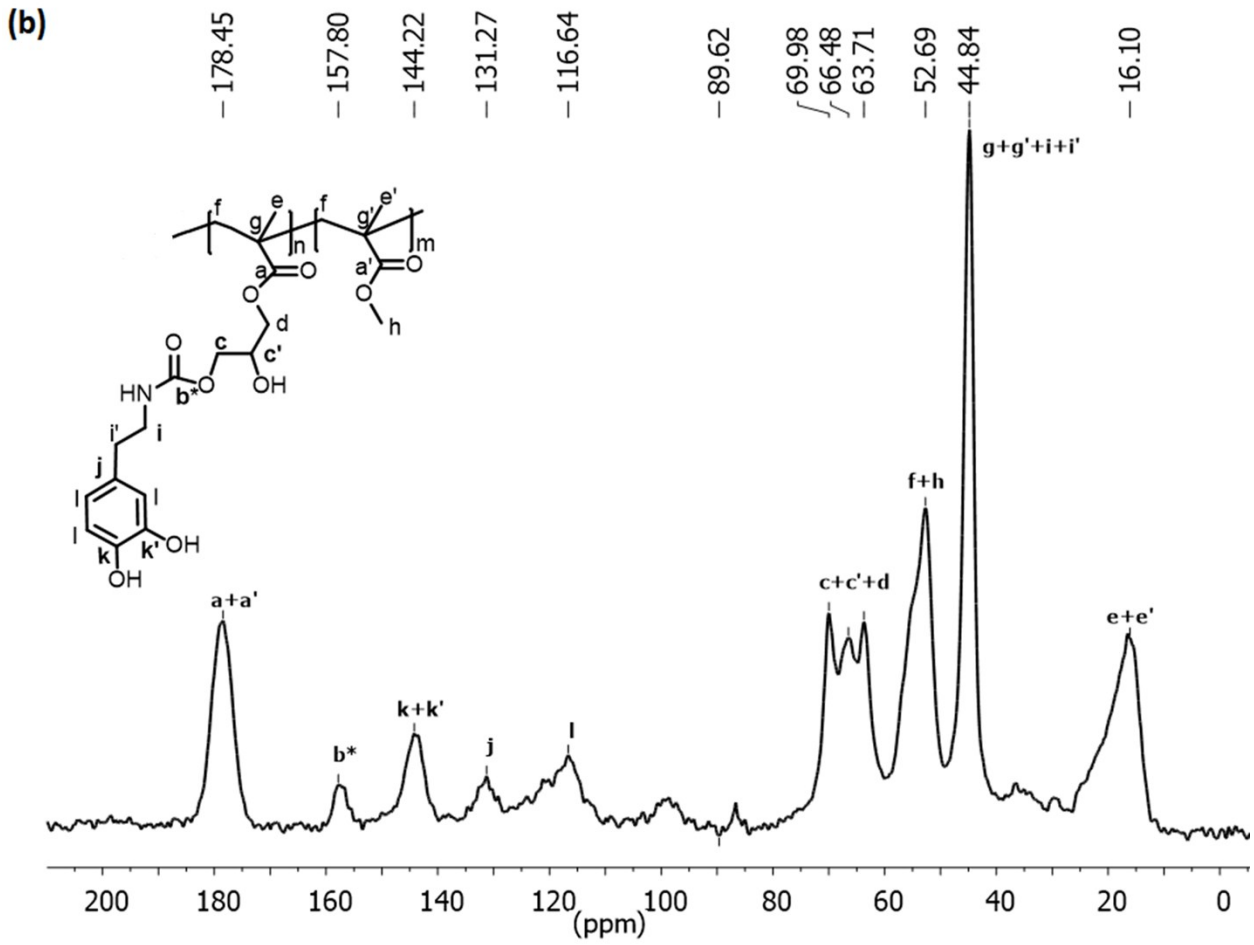
(b)
178.45
157.80
144.22
131.27
116.64
89.62
69.98
66.48
63.71
52.69
44.84
16.10
g+g'+i+i'
f+h
c+c'+d
e+e'
a+a'
k+k'
b*
j
l
200
180
160
140
120
100
80
60
40
20
0
(ppm)

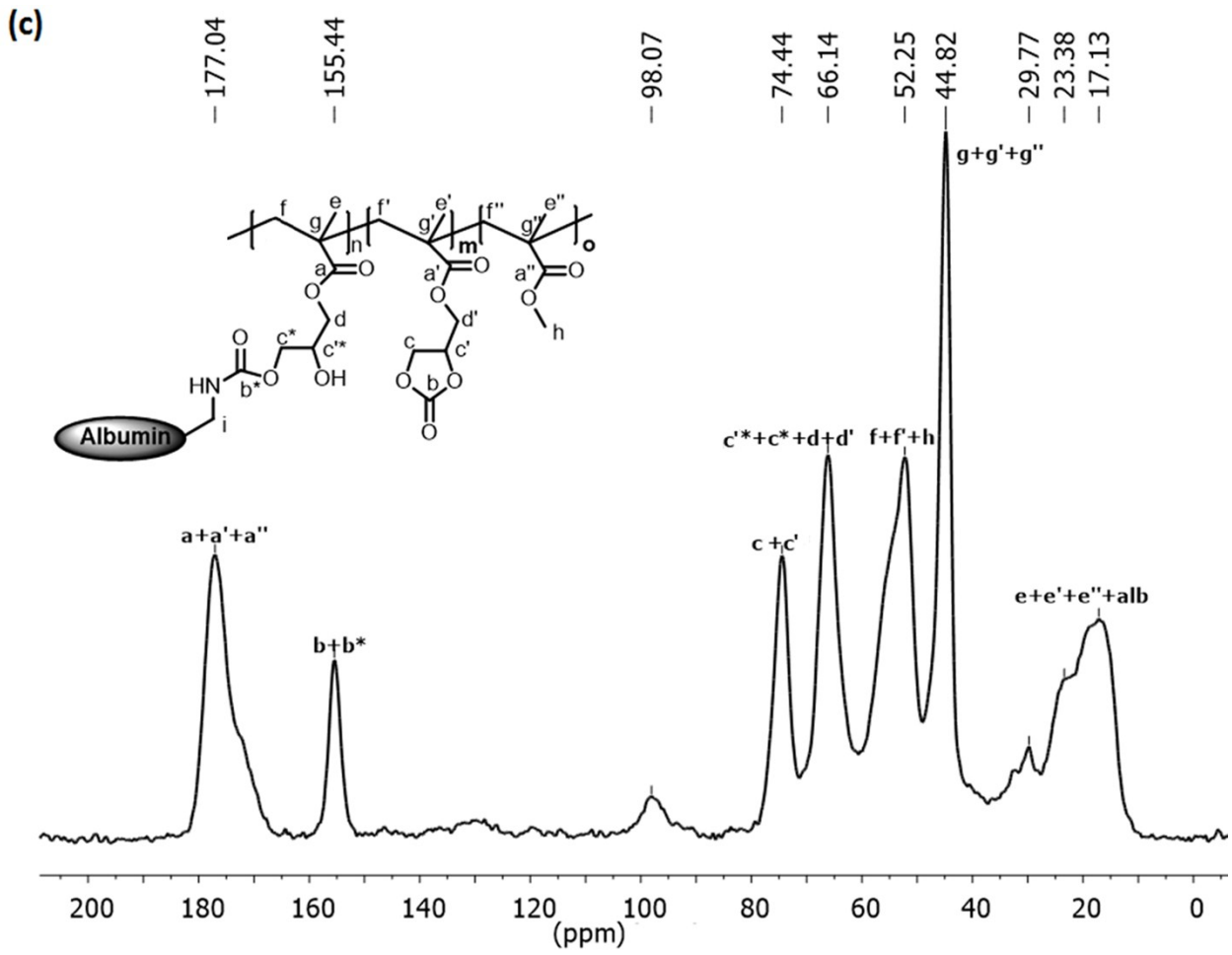
(c)
177.04
155.44
98.07
74.44
66.14
52.25
44.82
29.77
23.38
17.13
g+g'+g''
c'*+c*+d+d'
f+f'+h
a+a'+a''
c+c'
e+e'+e''+alb
b+b*
Albumin
200
180
160
140
120
100
80
60
40
20
0
(ppm)

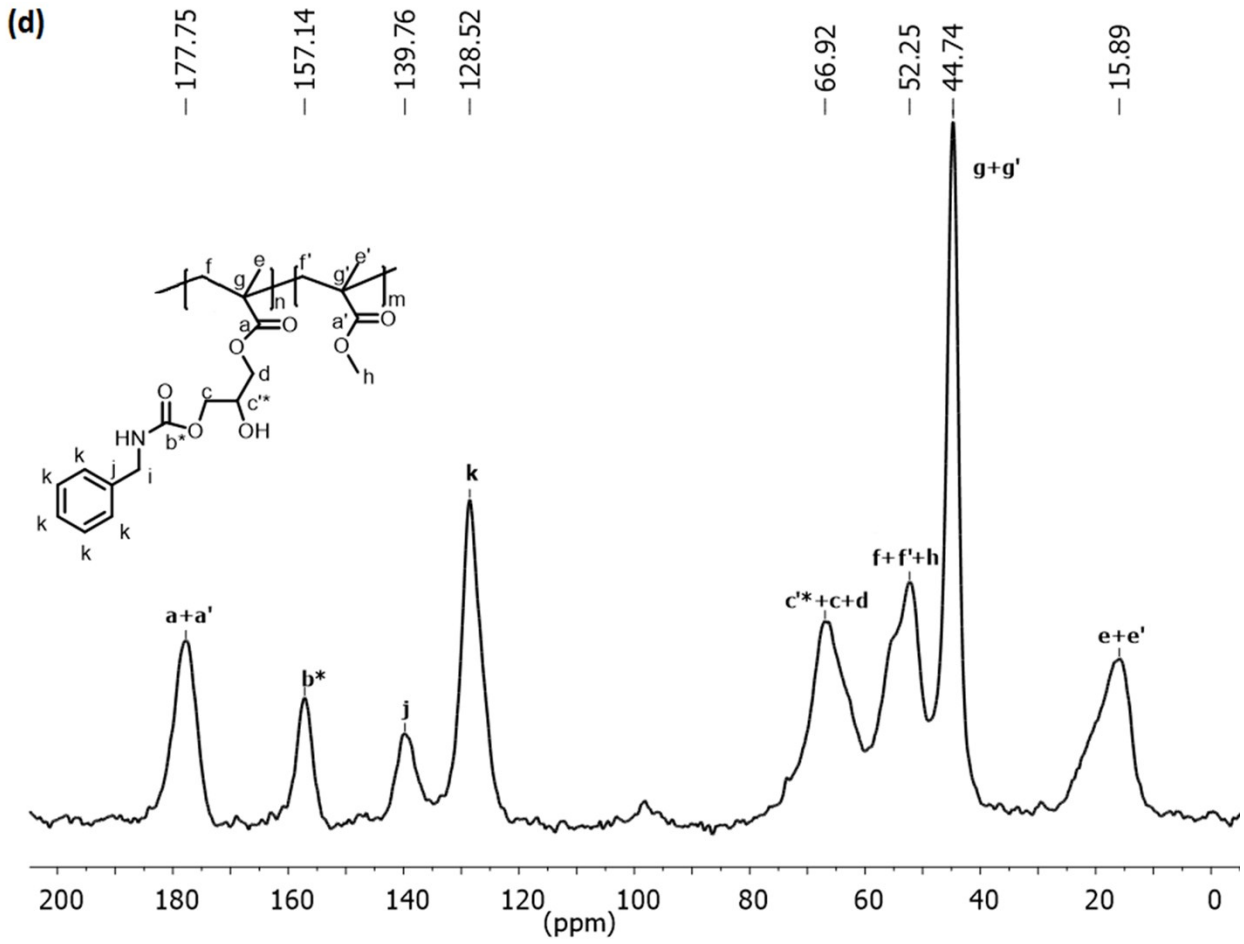
(d)
177.75
157.14
139.76
128.52
66.92
52.25
44.74
15.89
a+a'
b*
j
k
c'*+c+d
f+f'+h
g+g'
e+e'
200
180
160
140
120
100
80
60
40
20
0
(ppm)

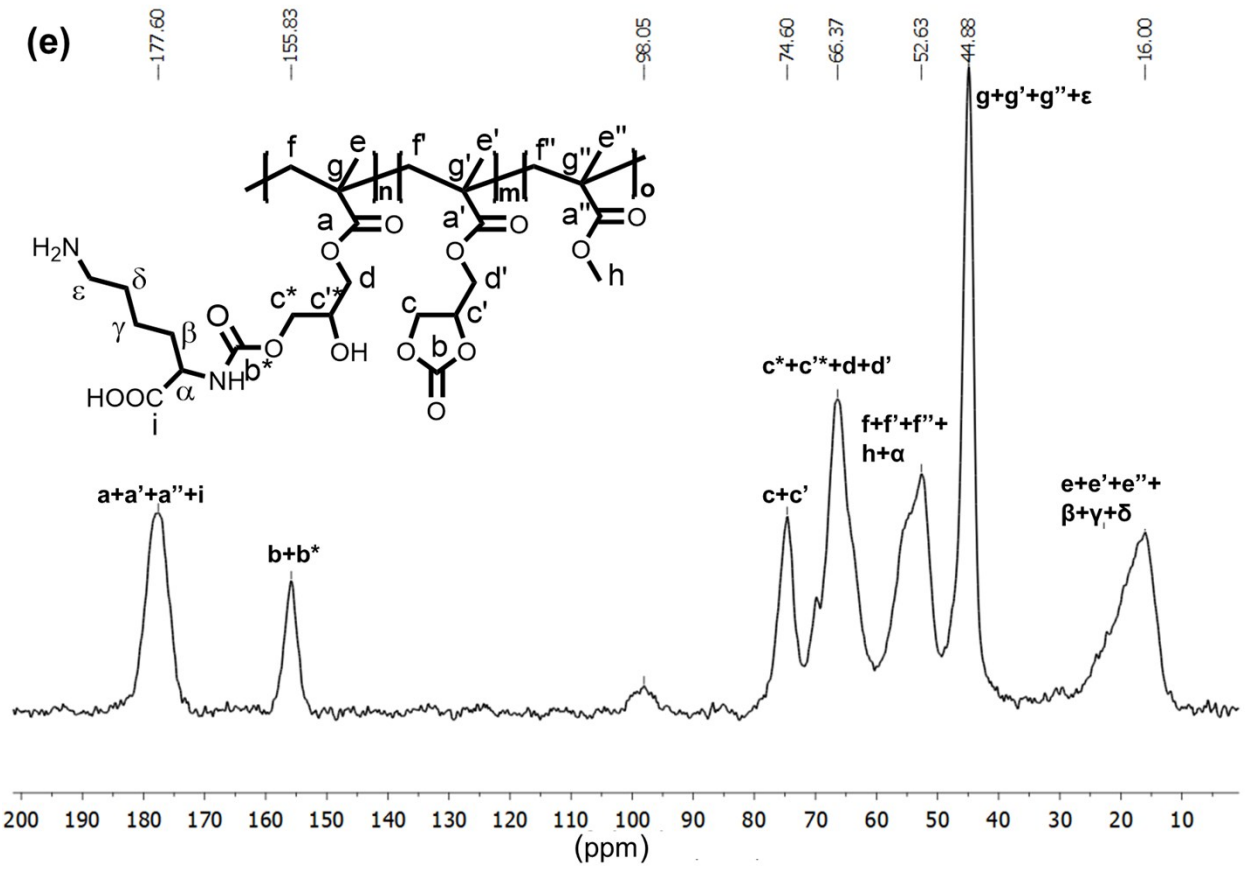

Figure S8. Solid state CP/MAS ^{13}C NMR spectra of purified and dried P(GCMA-co-MMA) nanoparticles (a); P-Dop (b); P-Alb 3; (c) P-BA 3 (d) and P-Lys 2 (e).

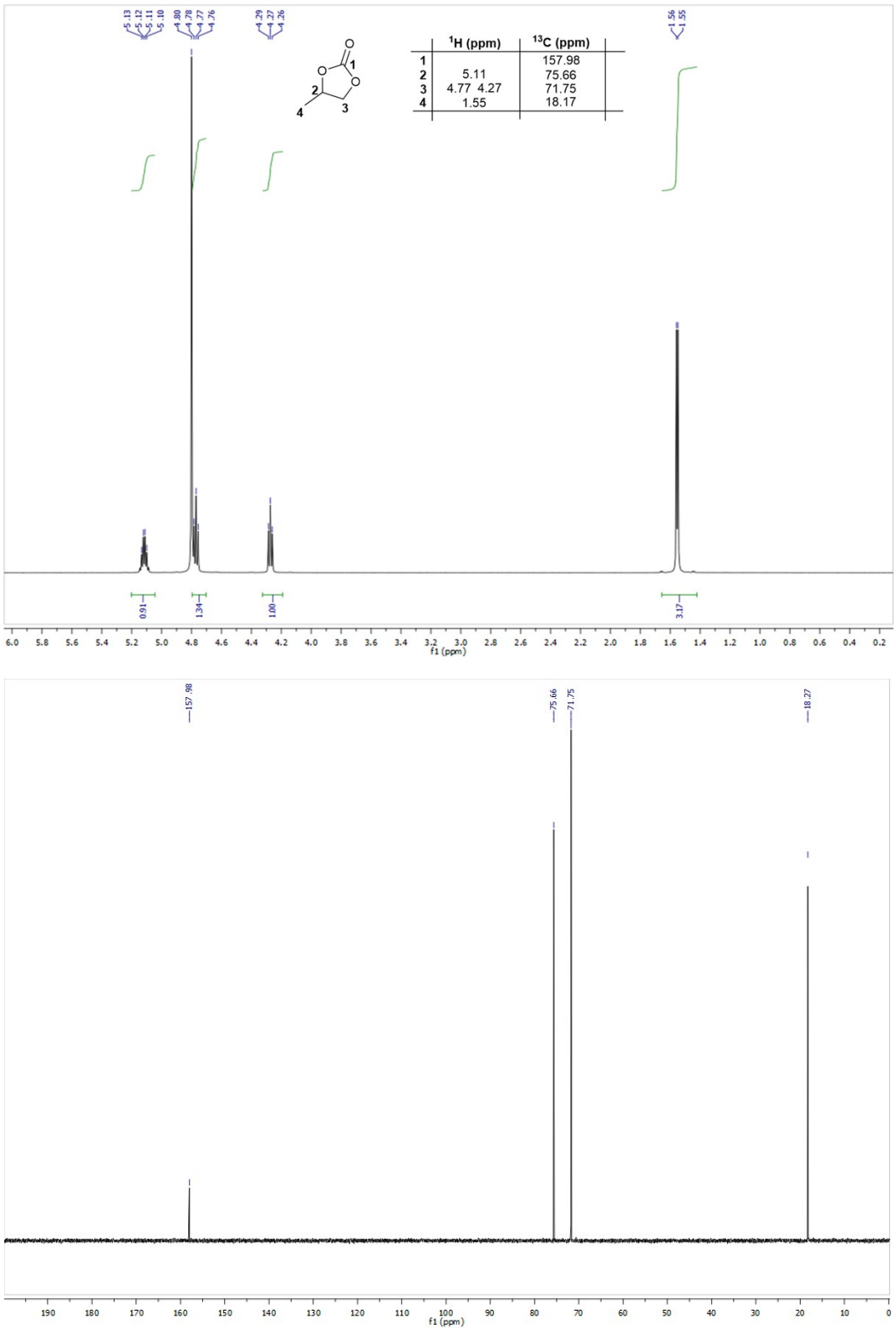

	^{1}H (ppm)	^{13}C (ppm)
1		157.98
2	5.11	75.66
3	4.77 4.27	71.75
4	1.55	18.17

Figure S9. ^{1}H (Top) and ^{13}C (Bottom) NMR spectra of propylene carbonate in D_2O.

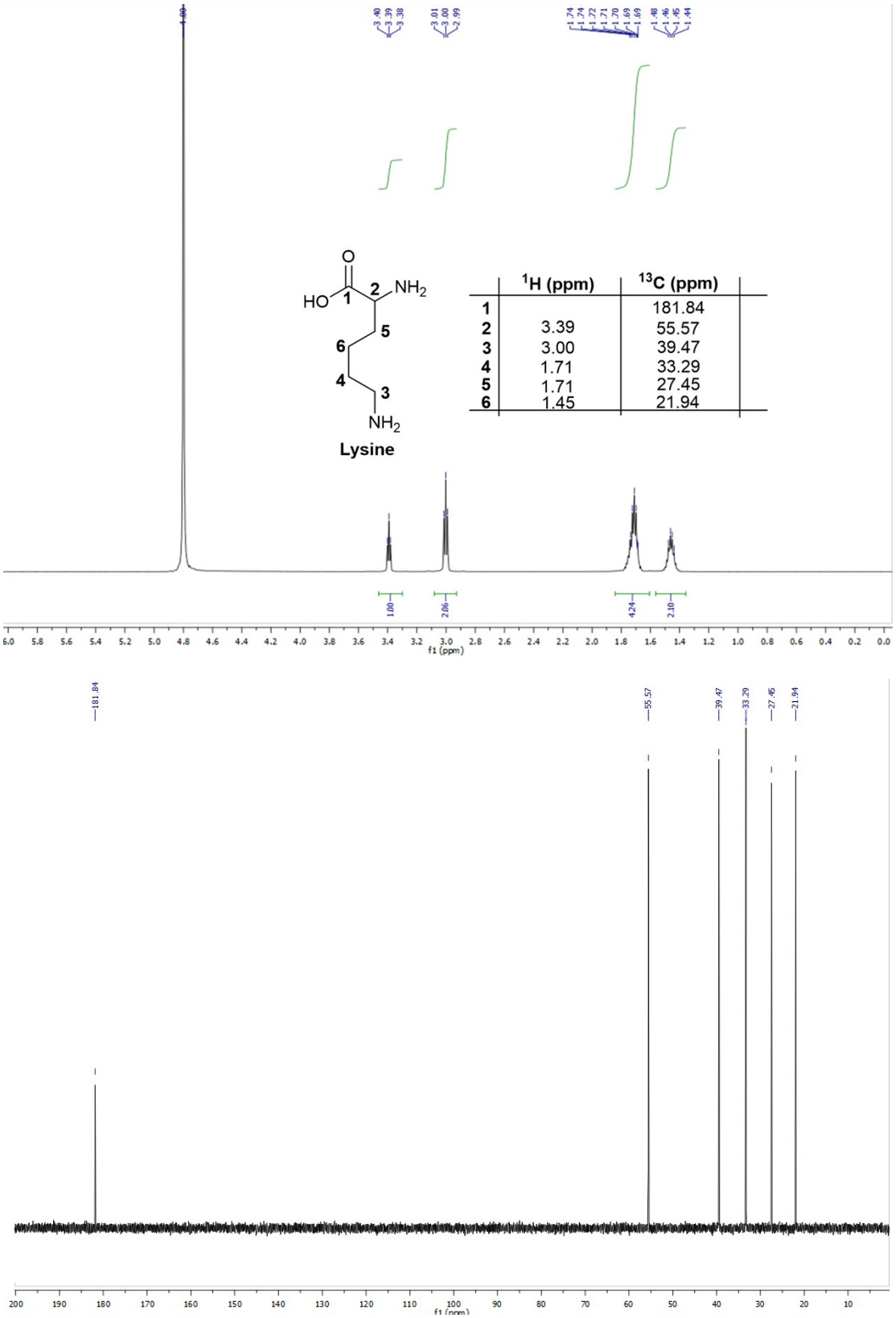

Figure S10. ^{1}H (Top) and ^{13}C (Bottom) NMR spectra of L-lysine in D_2O.

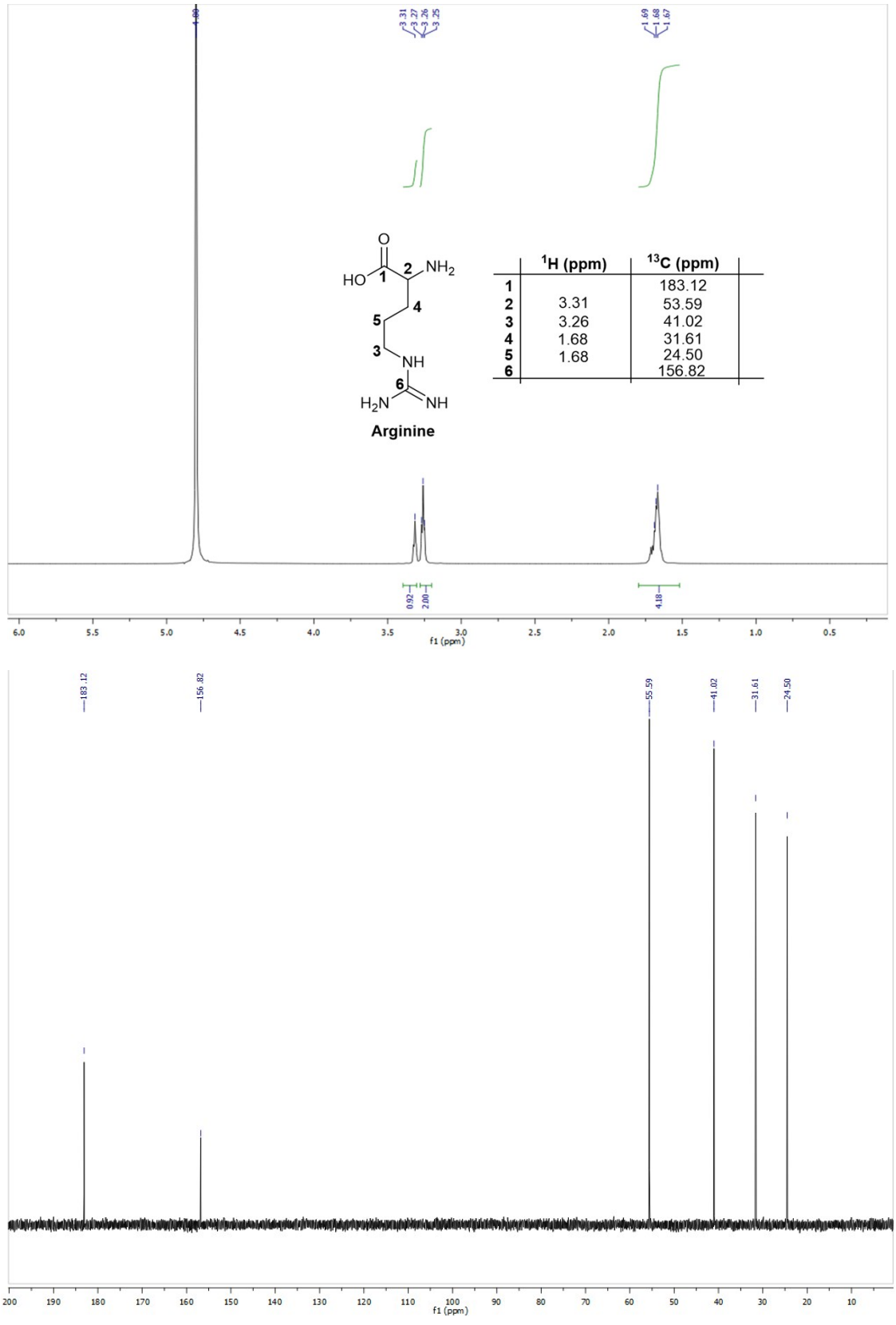

Figure S11. ^{1}H (Top) and ^{13}C (Bottom) NMR spectra of L-arginine in D_2O.

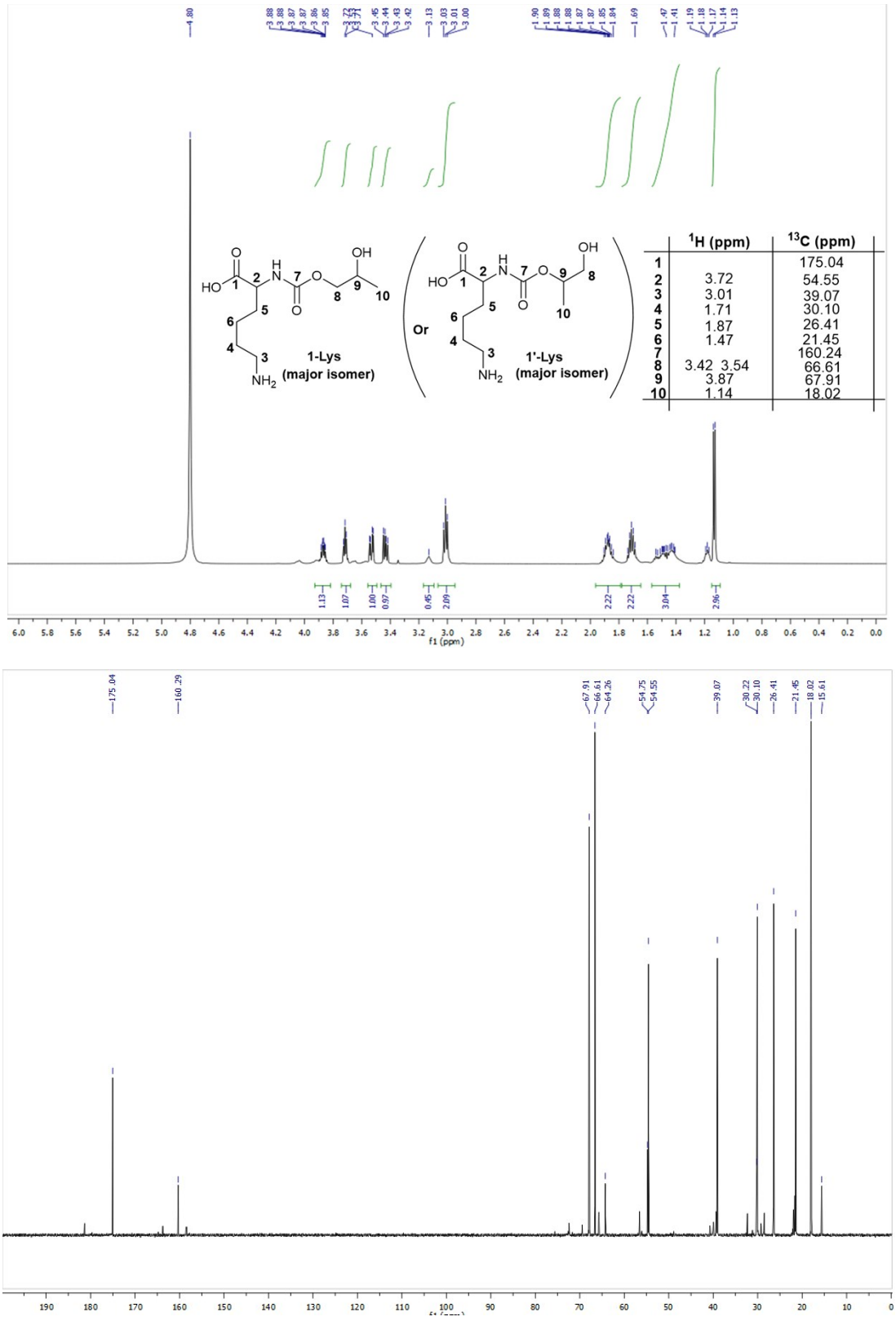

	^{1}H (ppm)	^{13}C (ppm)
1		175.04
2	3.72	54.55
3	3.01	39.07
4	1.71	30.10
5	1.87	26.41
6	1.47	21.45
7		160.24
8	3.42 3.54	66.61
9	3.87	67.91
10	1.14	18.02

Figure S12. ^{1}H (Top) and ^{13}C (Bottom) NMR spectra of **1-Lys** in D_2O.

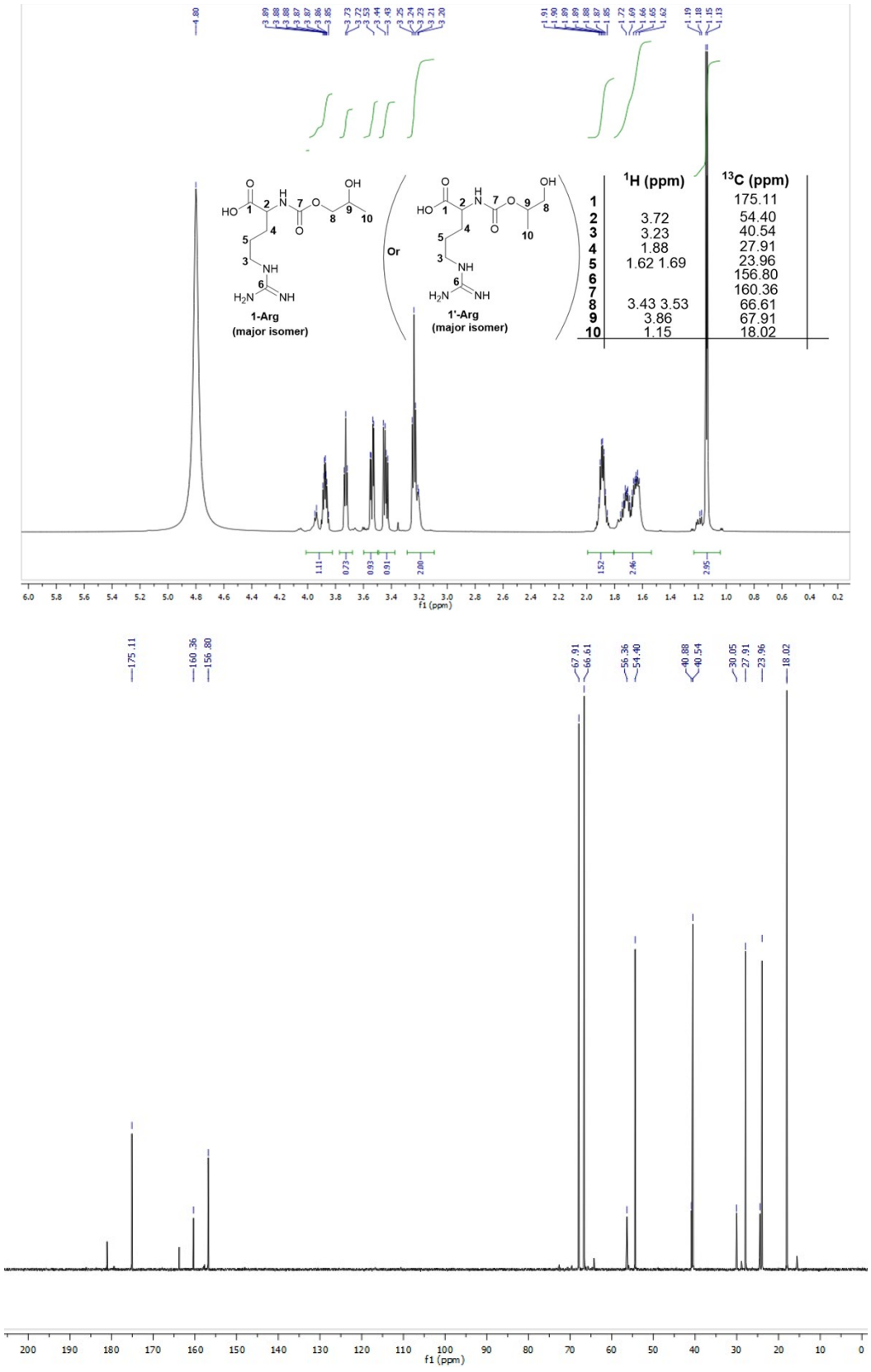

Figure S13. ^{1}H (Top) and ^{13}C (Bottom) NMR spectra of **1-Arg** in D_2O.

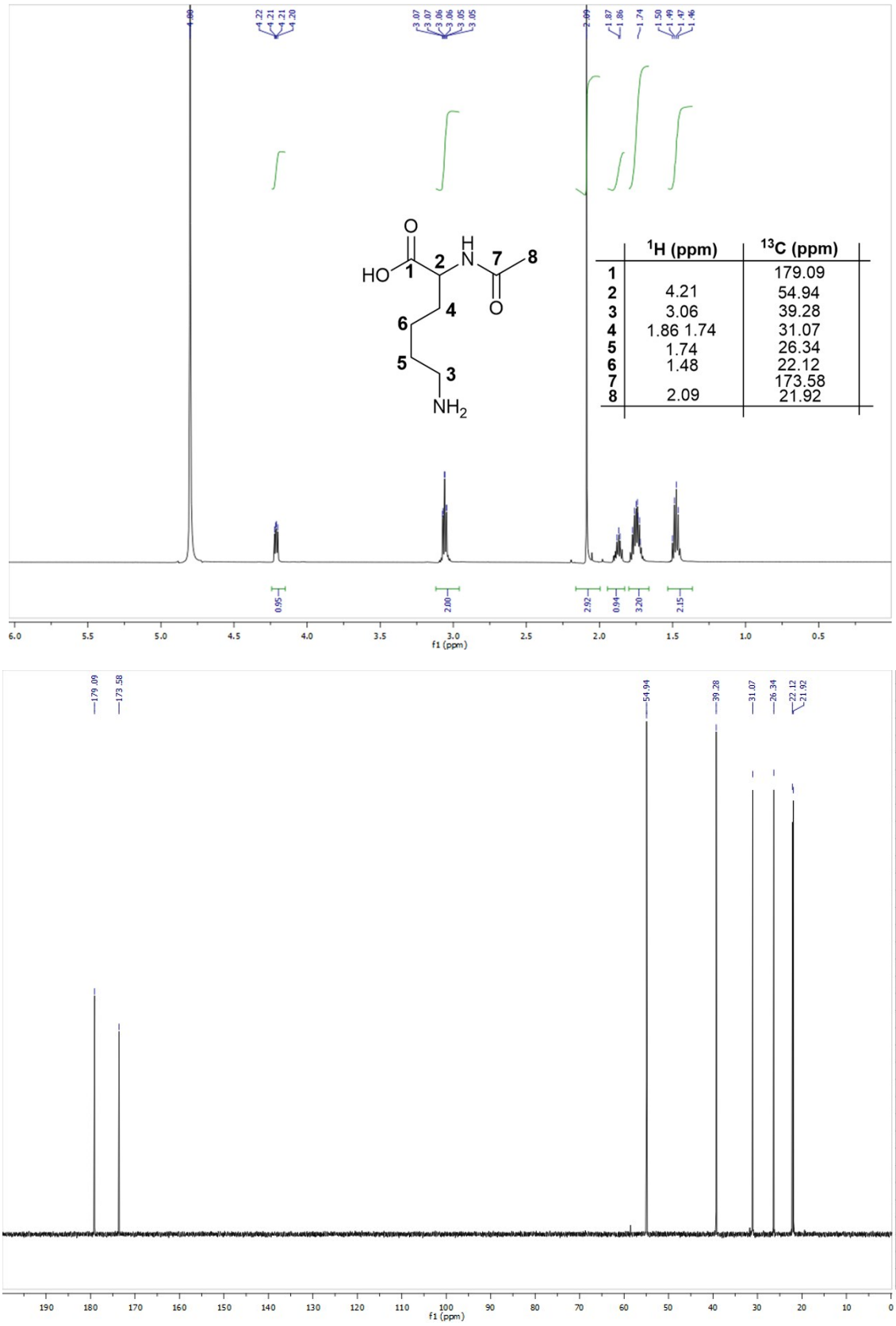

Figure S14. ^{1}H (Top) and ^{13}C (Bottom) NMR spectra of *N*-Ac-lysine in D_2O.

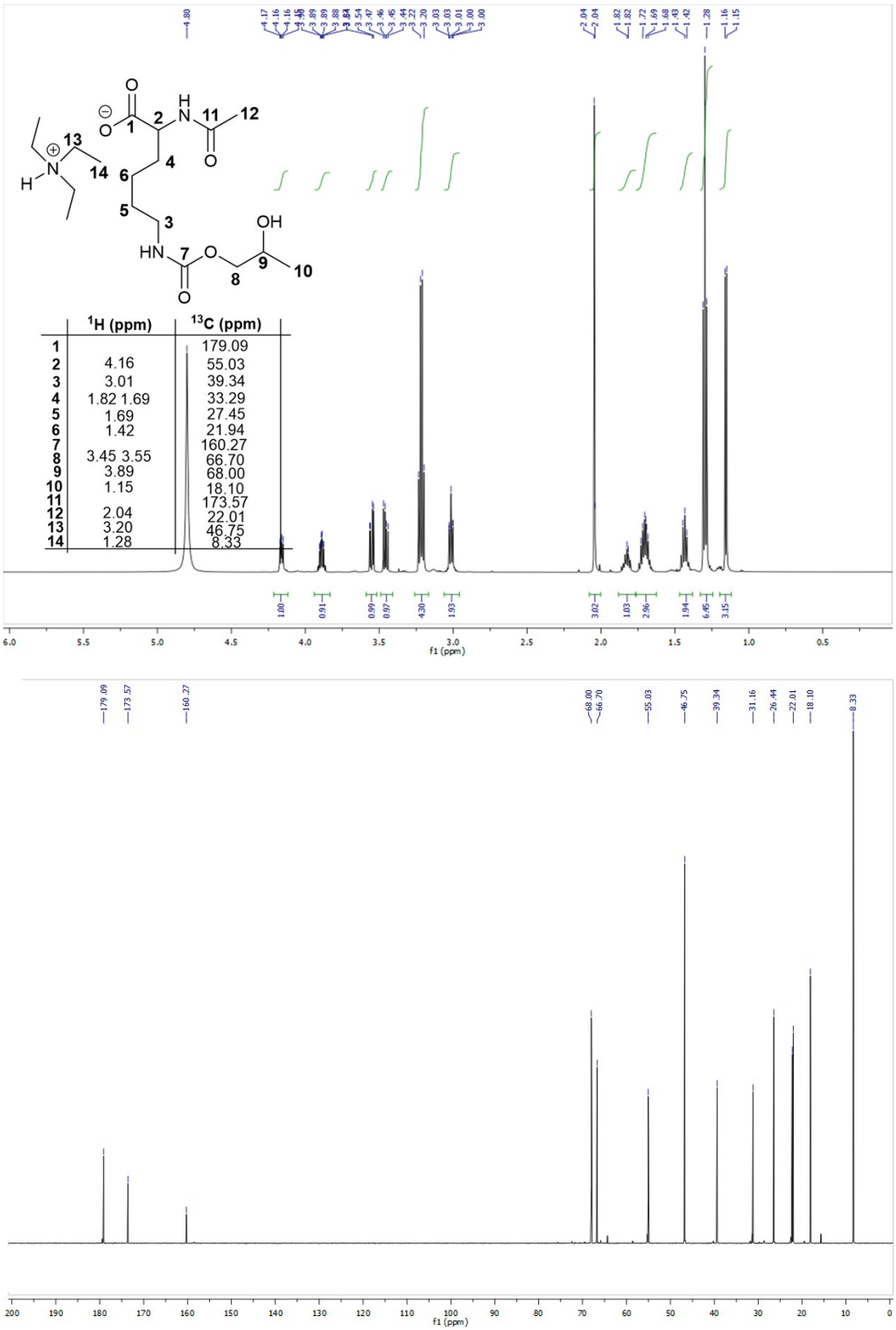

Figure S15. ^{1}H (Top) and ^{13}C (Bottom) NMR spectra of the product of the reaction of *N*-Ac-lysine with PC in presence of TEA (D_2O).

Table S3. Binding energies (eV) of C 1s components evaluated by deconvolution of high resolution XPS spectra of functionalized P(GCMA-*co*-MMA) nanoparticles.

Functional Group / Compound	C-C, C-H **(C1)**	-C-C=O **(C2)**	C-O, C-N, $C\text{-}NH_3^+$, C_α amino acids **(C3)**	$-COO^-$	O=C-N, R-(C=O)-R **(C4)**	-O(C=O)O-, -O(C=O)NH, $-NH\text{-}(C(NH_2)_2)^+$ **(C5)**
P(GCMA-co-MMA)	284.59	285.37	286.85		288.70	290.43
P-BA 1	284.69	285.7	286.7		288.82	290.60
P-HMDA 1	284.7	285.69	286.67		288.81	
P-Dop	284.55	285.57	286.50		288.79	
Arginine	284.58	285.22	286.41	287.25	288.77	
P-Arg 2	284.59	285.26	286.53	287.54	288.90	
P-Lys 2	284.51	285.16	286.34	287.31	288.83	
Albumin	284.76		286.19		287.93	
P-Alb 1	284.66	285.89	286.99		288.53	290.56
P-Alb 3	284.58	285.36	286.52		288.27	290.75

Table S4. Binding energies (eV) of N 1s components evaluated by deconvolution of high resolution XPS spectra of functionalized P(GCMA-*co*-MMA) nanoparticles.

Chemical Environment / **Compound**	-C-NH **(N1)**	O=C-NH **(N2)**	-O(C=O)NH -NH-$(C(NH_2)_2)^+$ **(N3)**	-NH_3^+ **(N4)**
P(GCMA-co-MMA)				
P-BA 1			399.75	
P-HMDA 1			399.68	401.63
P-Dop			399.87	
Arginine	398.42		399.73	
P-Arg 2			399.23	
P-Lys 2			399.27	
Albumin	398.22	399.72		
P-Alb 1	398.14	399.27	399.94	
P-Alb 3	399.02	399.65	400.30	

Table S5. Binding energies (eV) of O 1s components evaluated by deconvolution of high resolution XPS spectra of functionalized P(GCMA-*co*-MMA) nanoparticles.

Chemical Environment / **Compound**	(O=C)-NH- -O-(C=O)-C- -O-(C=O)-NH- **(O1)**	-(C=O)OH -O-(C=O)-O- **(O2)**	-O-(C=O)-O- -O-(C=O)- -O-(C=O)-NH- -OH **(O3)**
P(GCMA-*co*-MMA)	531.80	532.61	533.78
P-BA 1	532.09		533.48
P-HMDA 1	532.01		533.33
P-Dop	532.16		533.24
P-Arg 2	532.12		533.40
P-Lys 2	532.11		533.39
Albumin	530.98	531.94	533.29
P-Alb 1	531.03	531.998	533.66
P-Alb 3	531.10	532.05	533.61

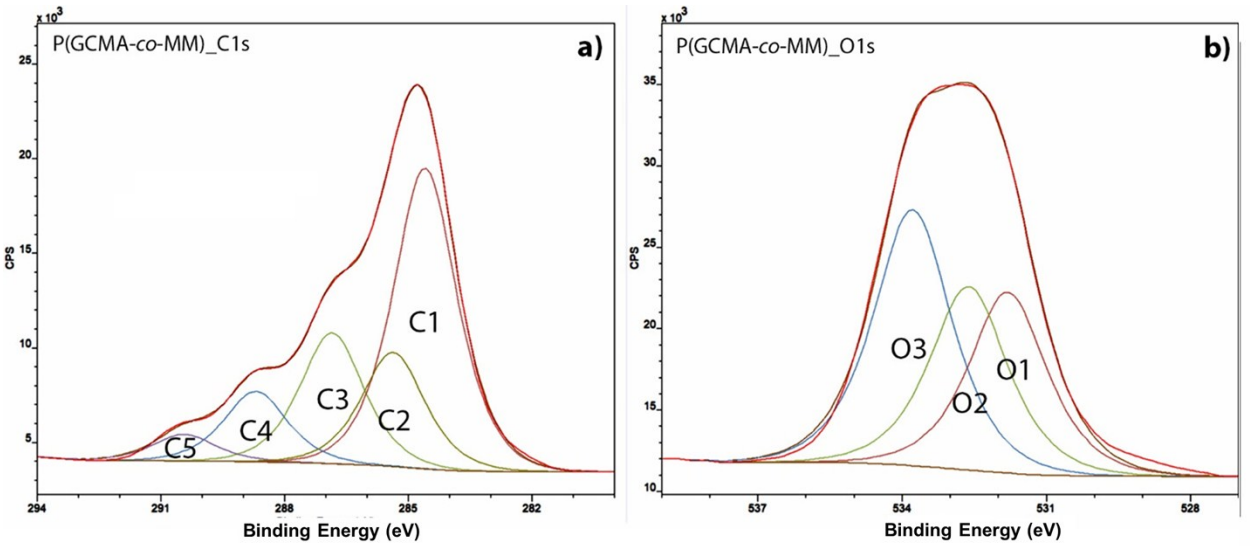

Figure S16. High resolution XPS spectra of P(GCMA-co-MMA) nanoparticles in the C 1s (a) and O 1s (b) spectral regions with components obtained by deconvolution.

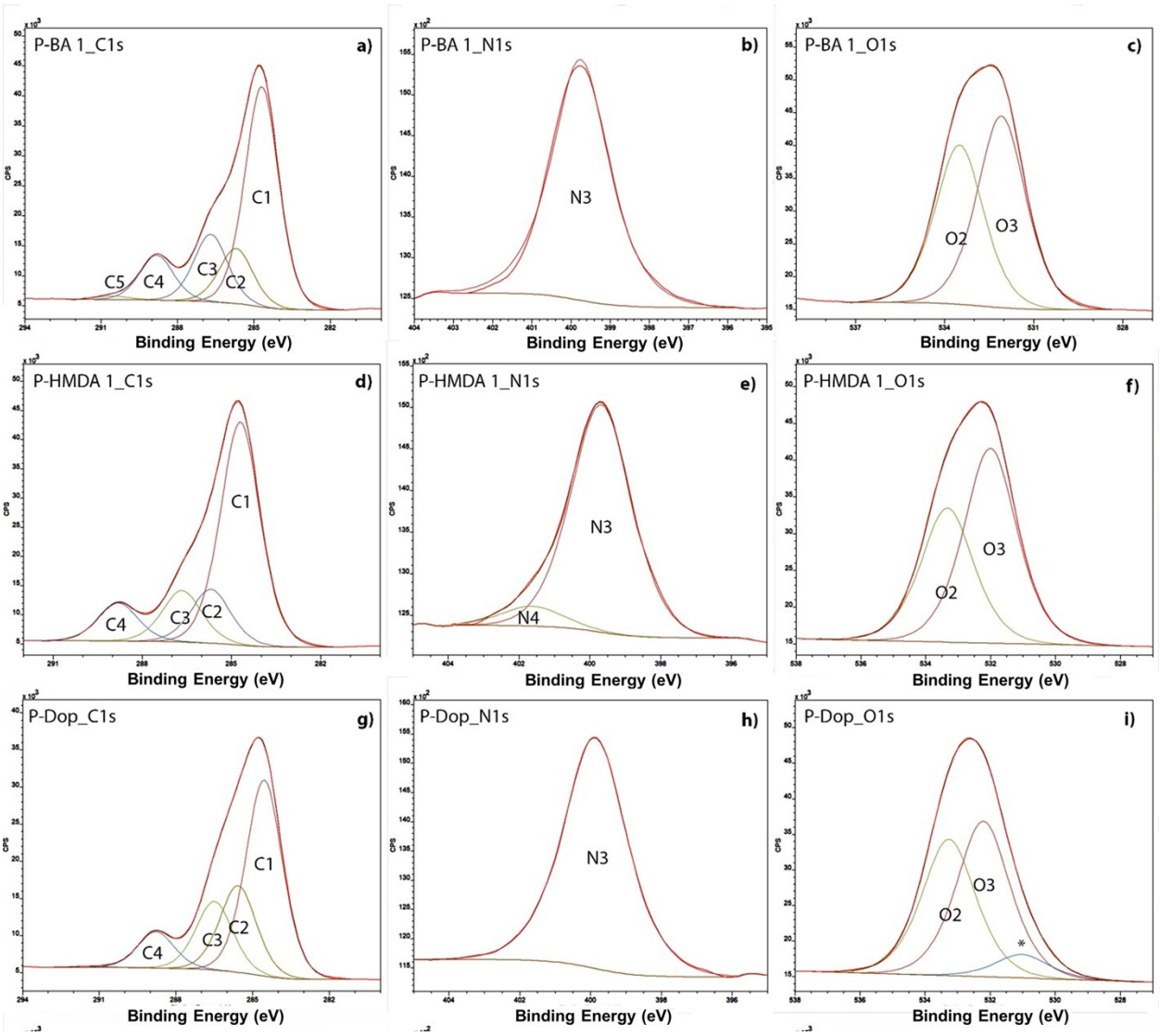
P-BA 1_C1s
a)
C1
C2
C3
C4
C5
Binding Energy (eV)
P-BA 1_N1s
b)
N3
Binding Energy (eV)
P-BA 1_O1s
c)
O2
O3
Binding Energy (eV)
P-HMDA 1_C1s
d)
C1
C2
C3
C4
Binding Energy (eV)
P-HMDA 1_N1s
e)
N3
N4
Binding Energy (eV)
P-HMDA 1_O1s
f)
O2
O3
Binding Energy (eV)
P-Dop_C1s
g)
C1
C2
C3
C4
Binding Energy (eV)
P-Dop_N1s
h)
N3
Binding Energy (eV)
P-Dop_O1s
i)
O2
O3
*
Binding Energy (eV)

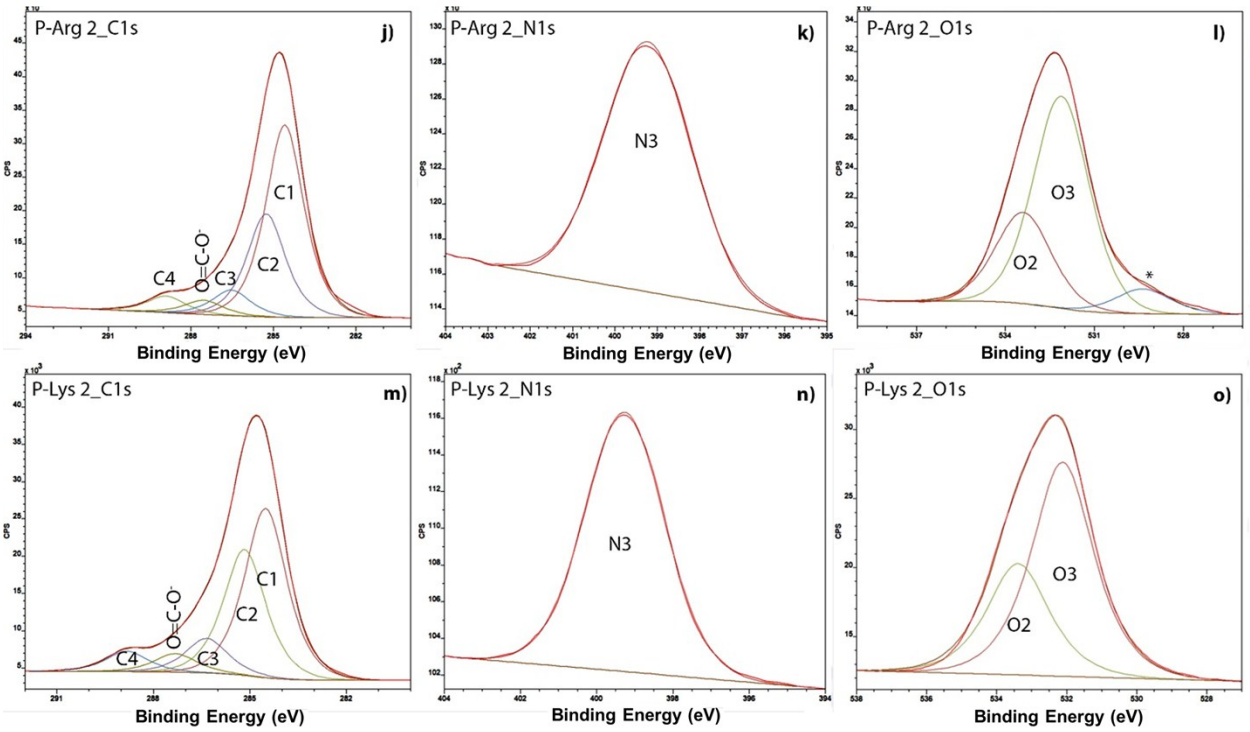

Figure S17. High resolution XPS spectra of P-BA 1 (a-c), P-HMDA 1, (d-f) P-Dop 1, (g-i) P-Arg 2, (j-l) and P-Lys 2 (m-o) in the C 1s, N 1s and O 1s spectral regions with components obtained by deconvolution. The O 1s fittings for P-Dop and P-Arg 2 include a minor component indicated by * that could be due to the presence of inorganic impurities.[1]

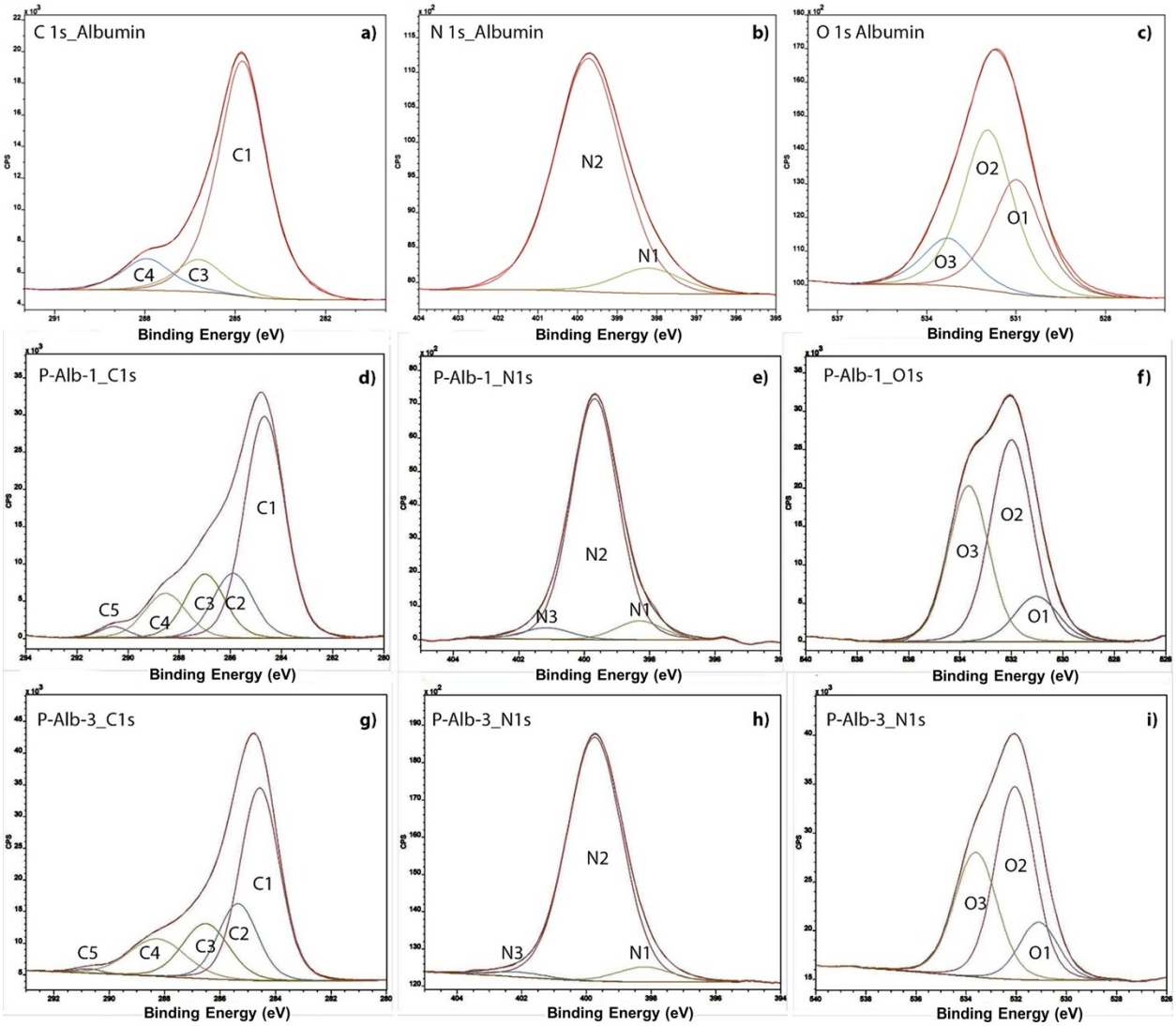

Figure S18. High resolution XPS spectra of pure albumin (a-c) and of P-Alb-1 (d-f) and P-Alb-3 (g-i) samples in the C 1s, N 1s and O 1s spectral regions with components obtained by deconvolution.

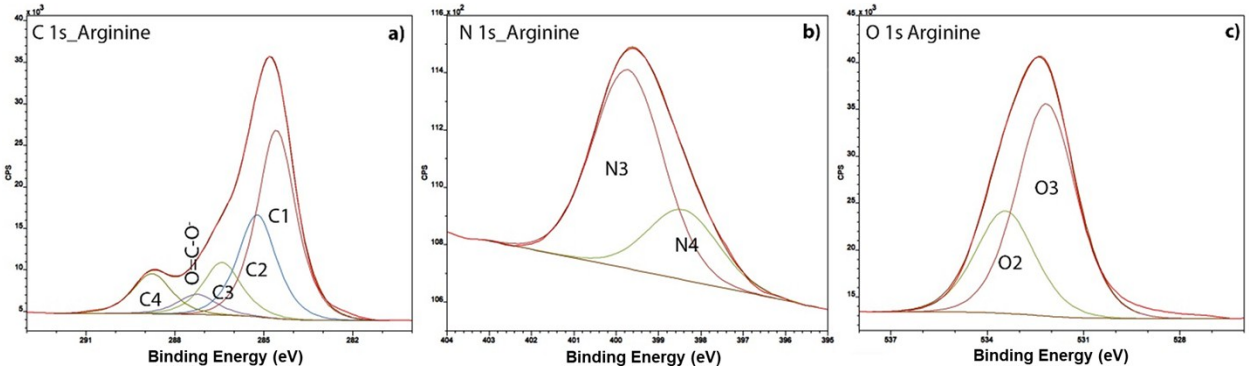

Figure S19. High resolution XPS spectra of arginine in the C 1s (a), N 1s (b) and O1s (c) spectral regions with components obtained by deconvolution.

Table S6. Atomic ratio of nitrogen to carbon measured by XPS for nanoparticles functionalized with several amines and albumin.

Entry	Amine/5CCs [mol%]	N/C (% molar ratio)
P-BA 1	50	3.0
P-HMDA 1	20	3.4
P-Dop	200	5.6
P-Arg 2	200	2.7
P-Lys 2	200	2.2
P-Alb 1	50[a]	7.7

[a] wt% albumin to P(GCMA-co-MMA) nanoparticles.

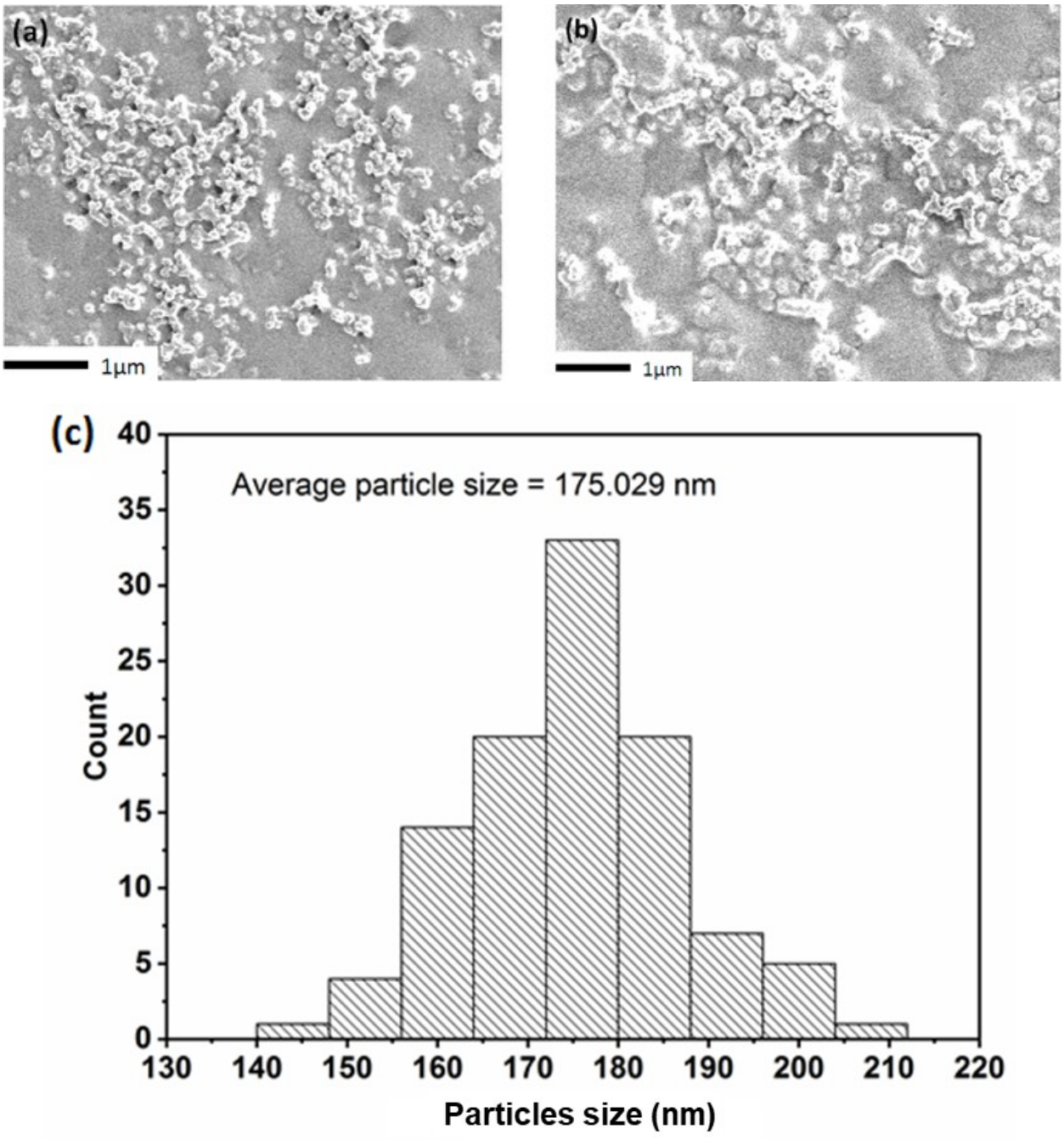

Figure S20. SEM micrographs of purified and dried P/Dop nanoparticles before catalysis (a); after catalysis (b); particle size of P-Dop determined from SEM measurements before catalysis (c).

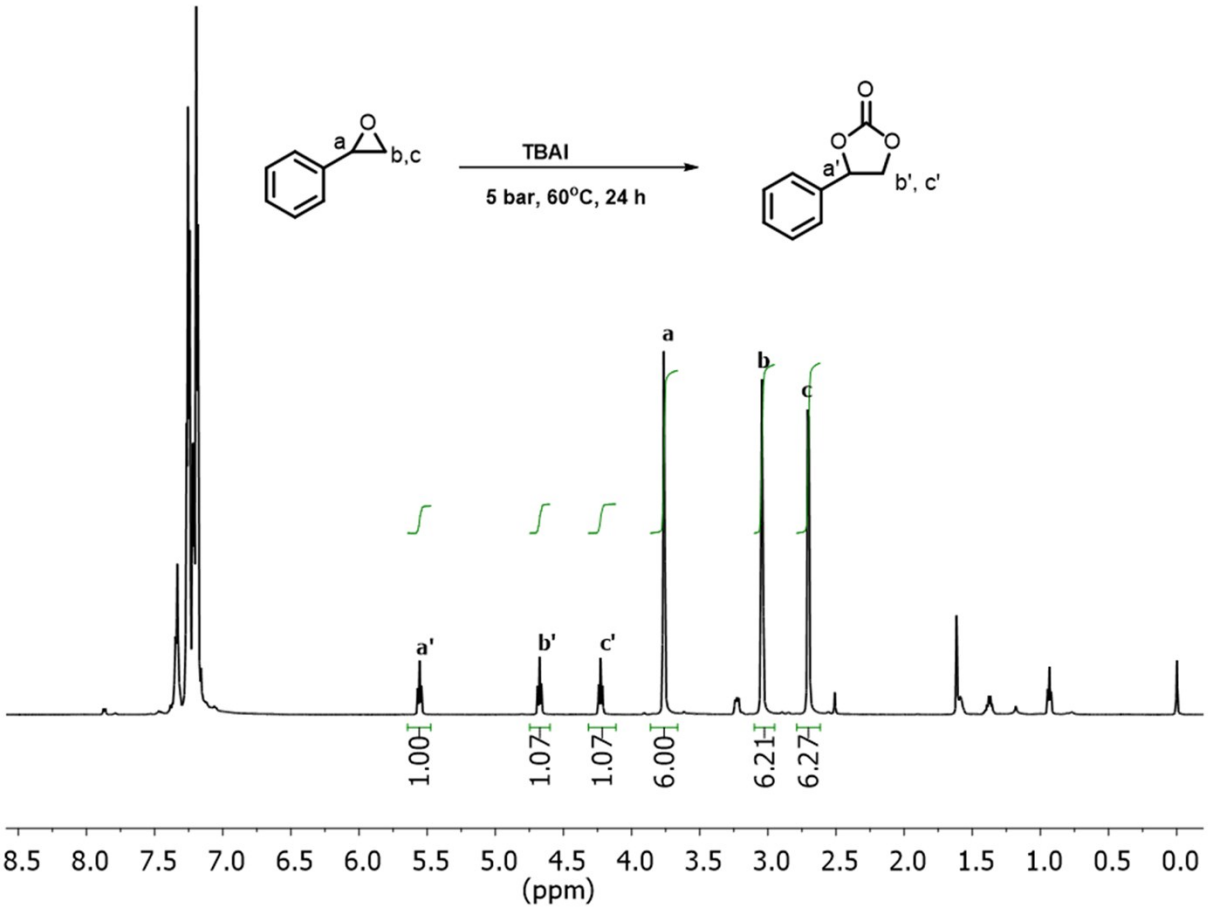

Figure S21. ^{1}H NMR spectrum of the products of the reaction between styrene oxide and CO_2 to afford styrene carbonate. The reaction is catalyzed by TBAI (Table 2, Entry 1). Additional peaks in the spectrum arise from residual $CHCl_3$ in the $CDCl_3$ (7.24 ppm), H_2O in $CDCl_3$ (1.6 ppm), TMS standard (0.0 ppm), and TBAI (3.26, 1.70, 1.35 and 0.9 ppm).

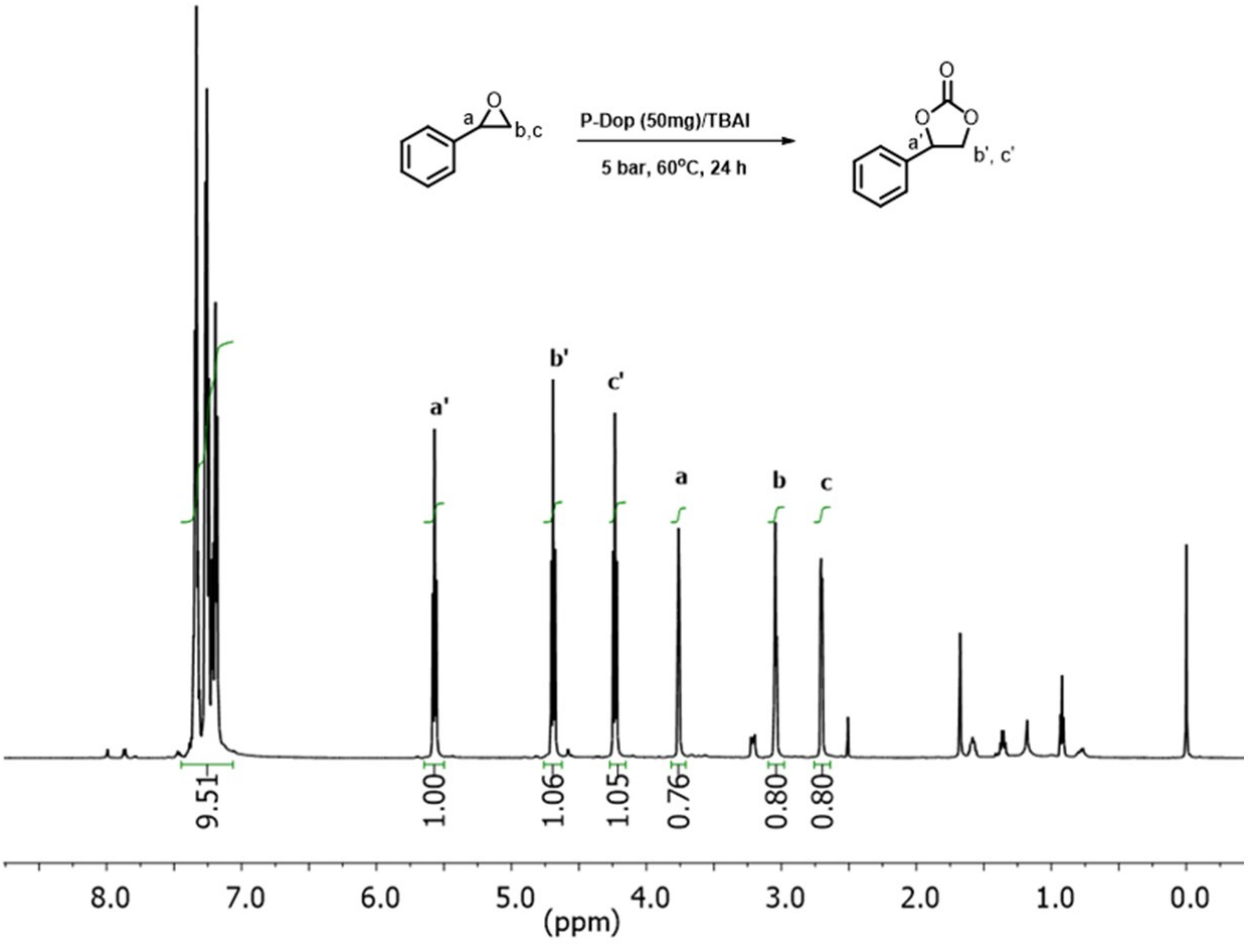

Figure S22. ^{1}H NMR spectrum of the product of the reaction between styrene oxide and CO_2 to afford styrene carbonate. The reaction is catalyzed by TBAI and 50 mg P-Dop (Table 2, Entry 4). Additional peaks in the spectrum arise from residual $CHCl_3$ in $CDCl_3$ (7.24 ppm), H_2O in $CDCl_3$ (1.6 ppm), TMS standard (0.0 ppm), and TBAI (3.26, 1.70, 1.35 and 0.9 ppm).

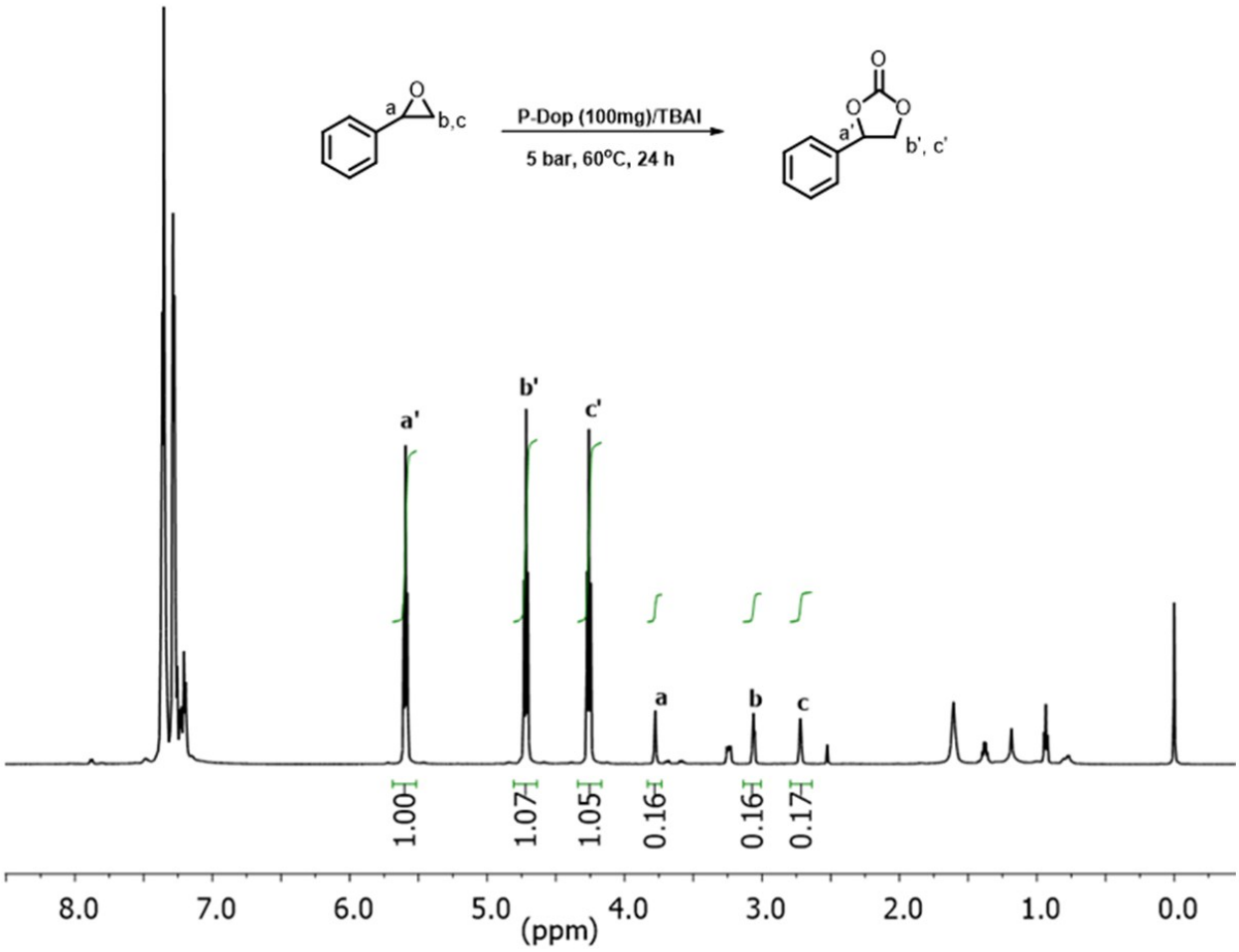

Figure S23. ^{1}H NMR spectrum of the product of the reaction between styrene oxide and CO_2 to afford styrene carbonate. The reaction is catalyzed by TBAI and 100 mg P-Dop (Table 2, Entry 5). Additional peaks in the spectrum arise from residual $CHCl_3$ in $CDCl_3$ (7.24 ppm), H_2O in $CDCl_3$ (1.6 ppm), TMS standard (0.0 ppm), and TBAI (3.26, 1.70, 1.35 and 0.9 ppm).

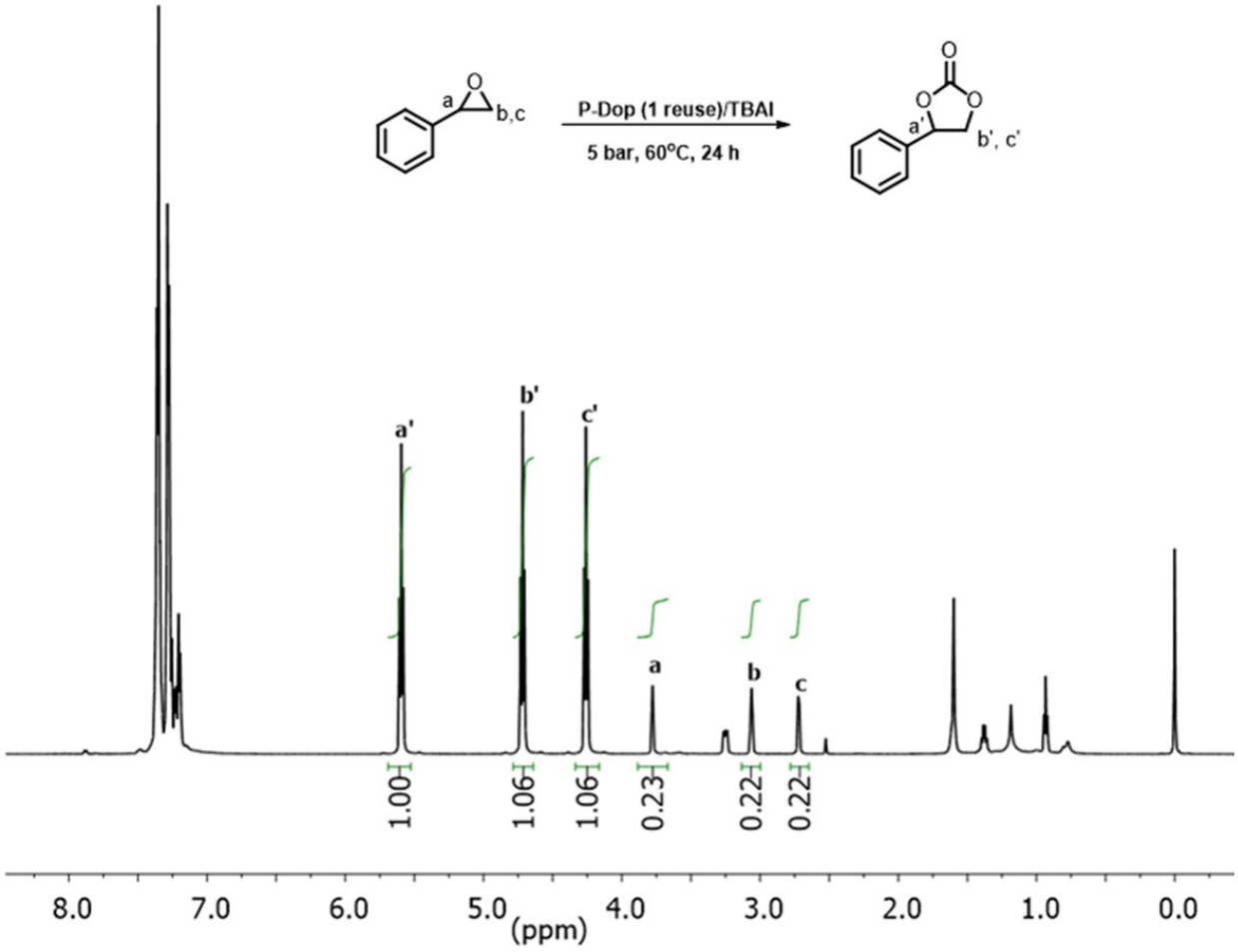

Figure S24. ^{1}H NMR spectrum of the product of the reaction between styrene oxide and CO_2 to afford styrene carbonate. The reaction is catalyzed by TBAI and recycled (1st time) P-Dop (Table 2, Entry 6). Additional peaks in the spectrum arise from residual $CHCl_3$ in $CDCl_3$ (7.24 ppm), H_2O in $CDCl_3$ (1.6 ppm), TMS standard (0.0 ppm), and TBAI (3.26, 1.70, 1.35 and 0.9 ppm).

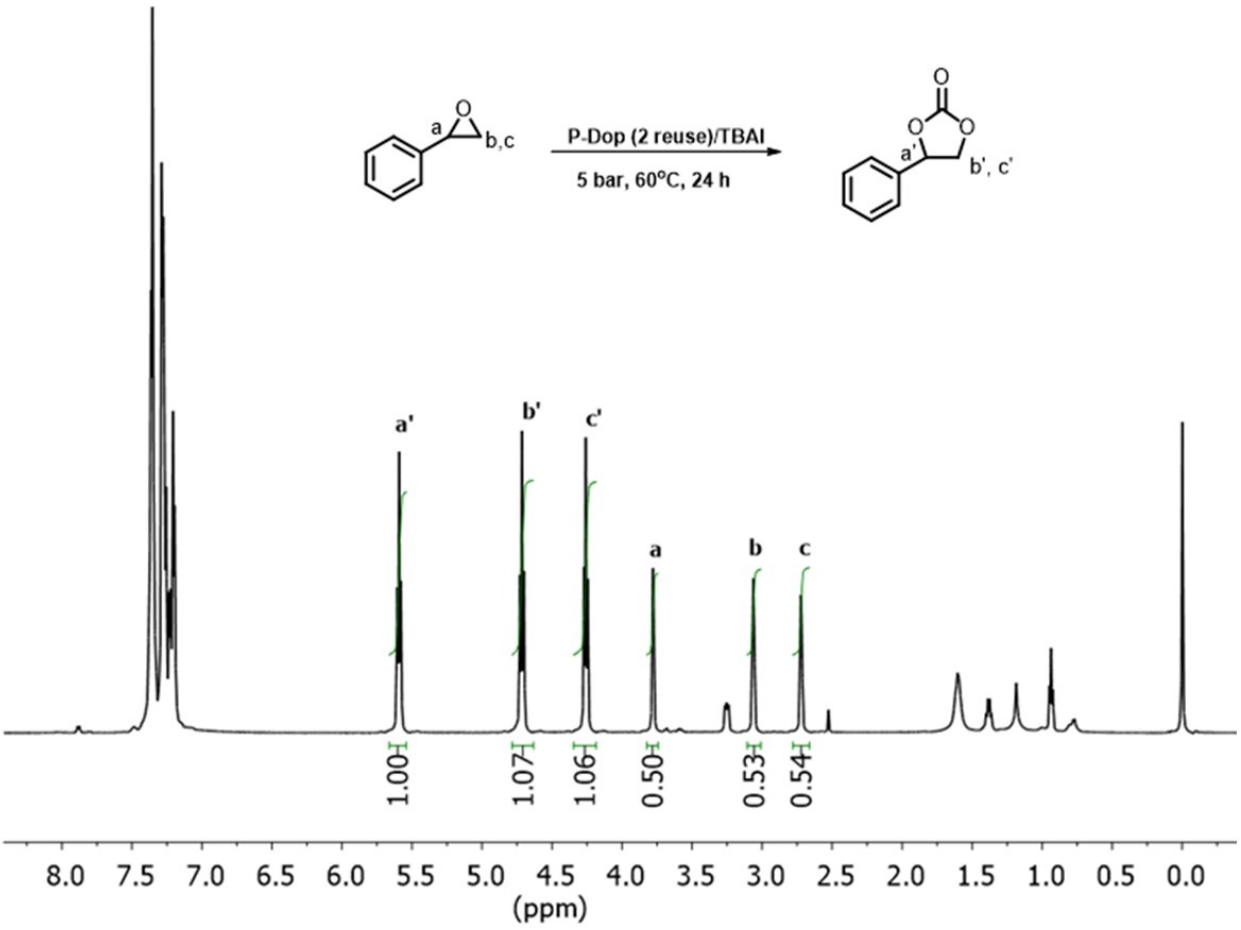

Figure S25. ^{1}H NMR spectrum of the product of the reaction between styrene oxide and CO_2 to afford styrene carbonate. The reaction is catalyzed by TBAI and recycled (2nd time) P-Dop (Table 2, Entry 7). Additional peaks in the spectrum arise from residual $CHCl_3$ in $CDCl_3$ (7.24 ppm), H_2O in $CDCl_3$ (1.6 ppm), TMS standard (0.0 ppm), and TBAI (3.26, 1.70, 1.35 and 0.9 ppm).

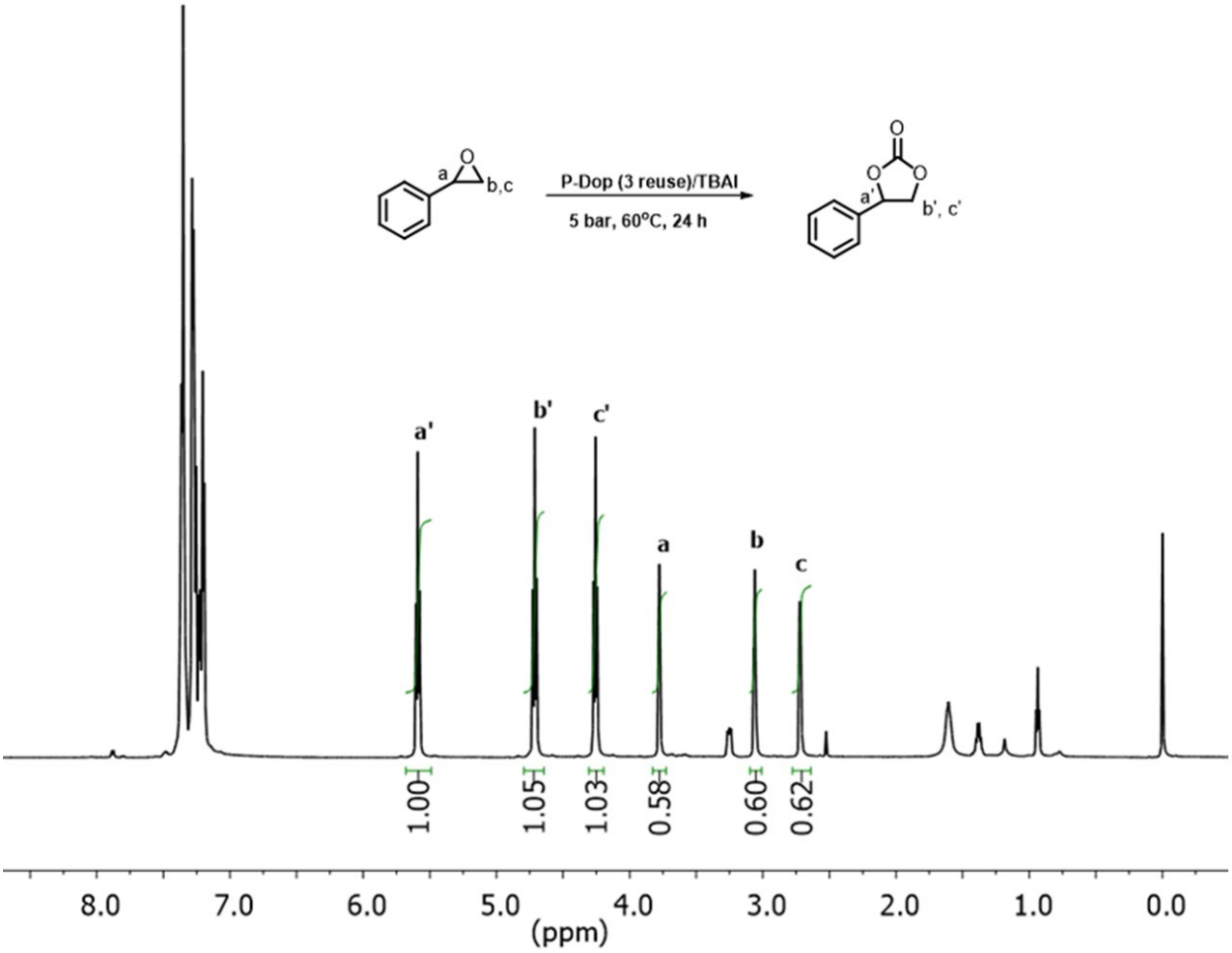

Figure S26. ^{1}H NMR spectrum of the product of the reaction between styrene oxide and CO_2 to afford styrene carbonate. The reaction is catalyzed by TBAI and recycled (3rd time) P-Dop (Table 2, Entry 8). Additional peaks in the spectrum arise from residual $CHCl_3$ in $CDCl_3$ (7.24 ppm), H_2O in $CDCl_3$ (1.6 ppm), TMS standard (0.0 ppm), and TBAI (3.26, 1.70, 1.35 and 0.9 ppm).

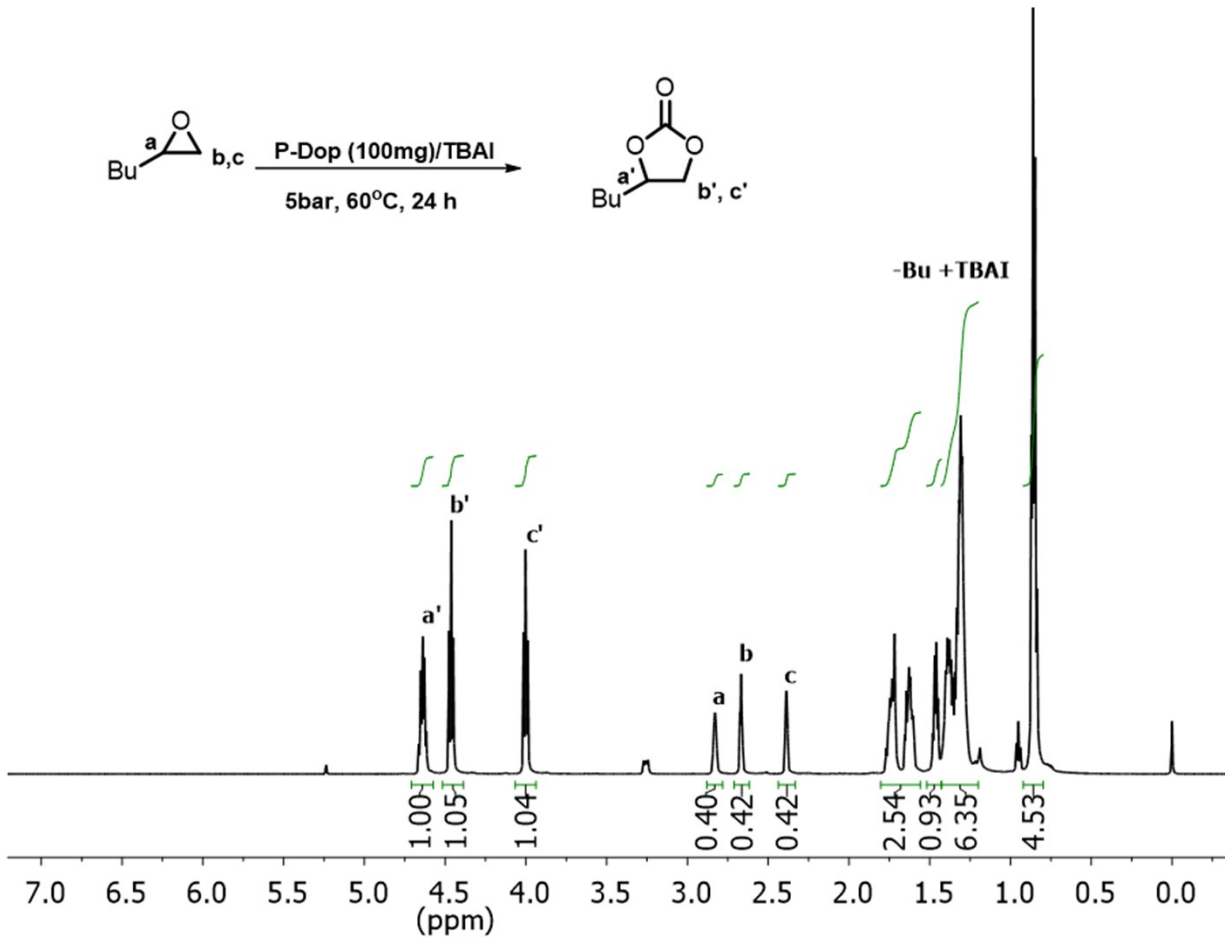

Figure S27. ^{1}H NMR spectrum of the product of the reaction between 1-hexene oxide and CO_2 to afford 1-hexene carbonate. The reaction is catalyzed by TBAI and P-Dop (Table 2, Entry 9). Additional peaks in the spectrum arise from residual $CHCl_3$ in $CDCl_3$ (7.24 ppm), TMS standard (0.0 ppm), and TBAI (3.26, 1.35 and 0.9 ppm).

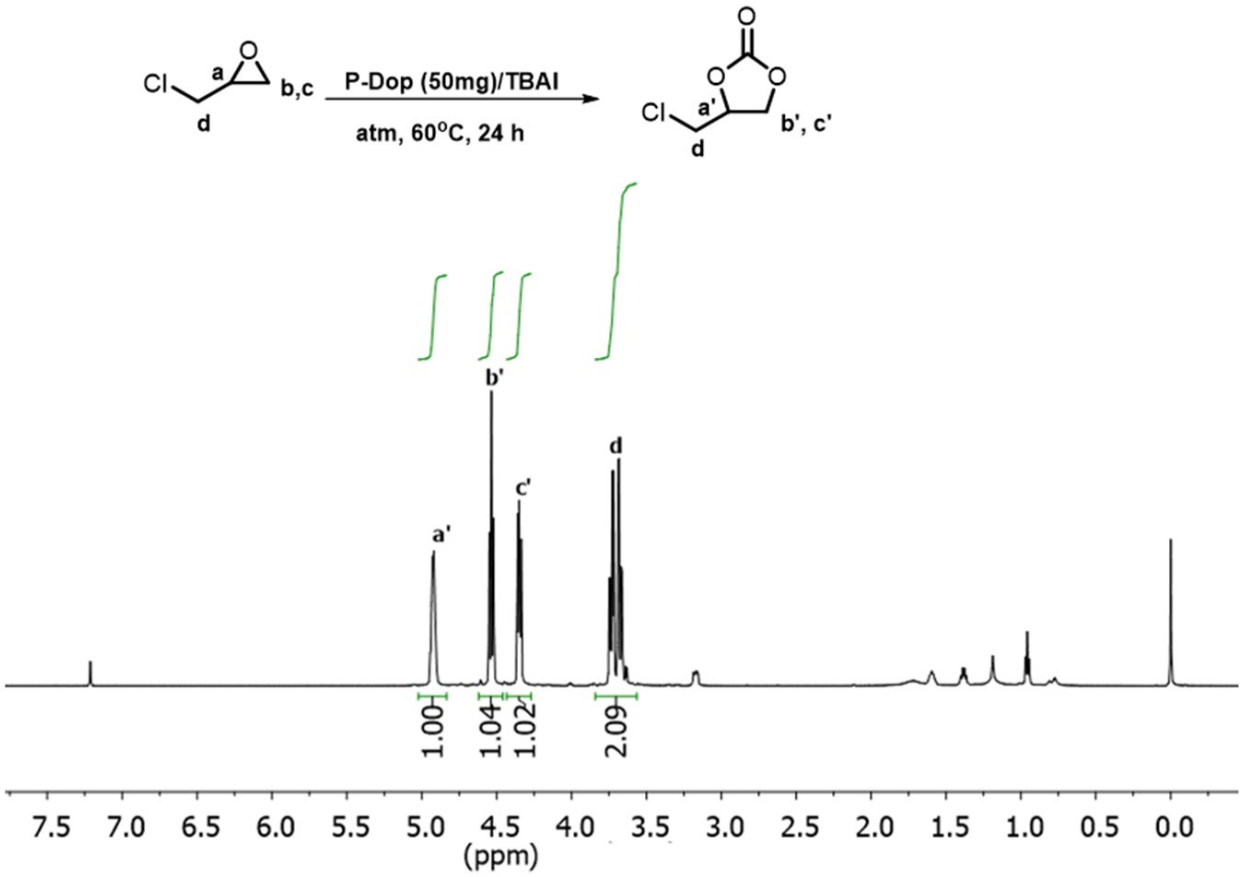

Figure S28 ^{1}H NMR spectrum of the product of the reaction between epichlorohydrin and CO_2 to afford epichlorohydrin carbonate. The reaction is catalyzed by TBAI and P-Dop (Table 2, Entry 10). Additional peaks in the spectrum arise from TMS standard (0.0 ppm) and TBAI (3.26, 1.35 and 0.9 ppm).

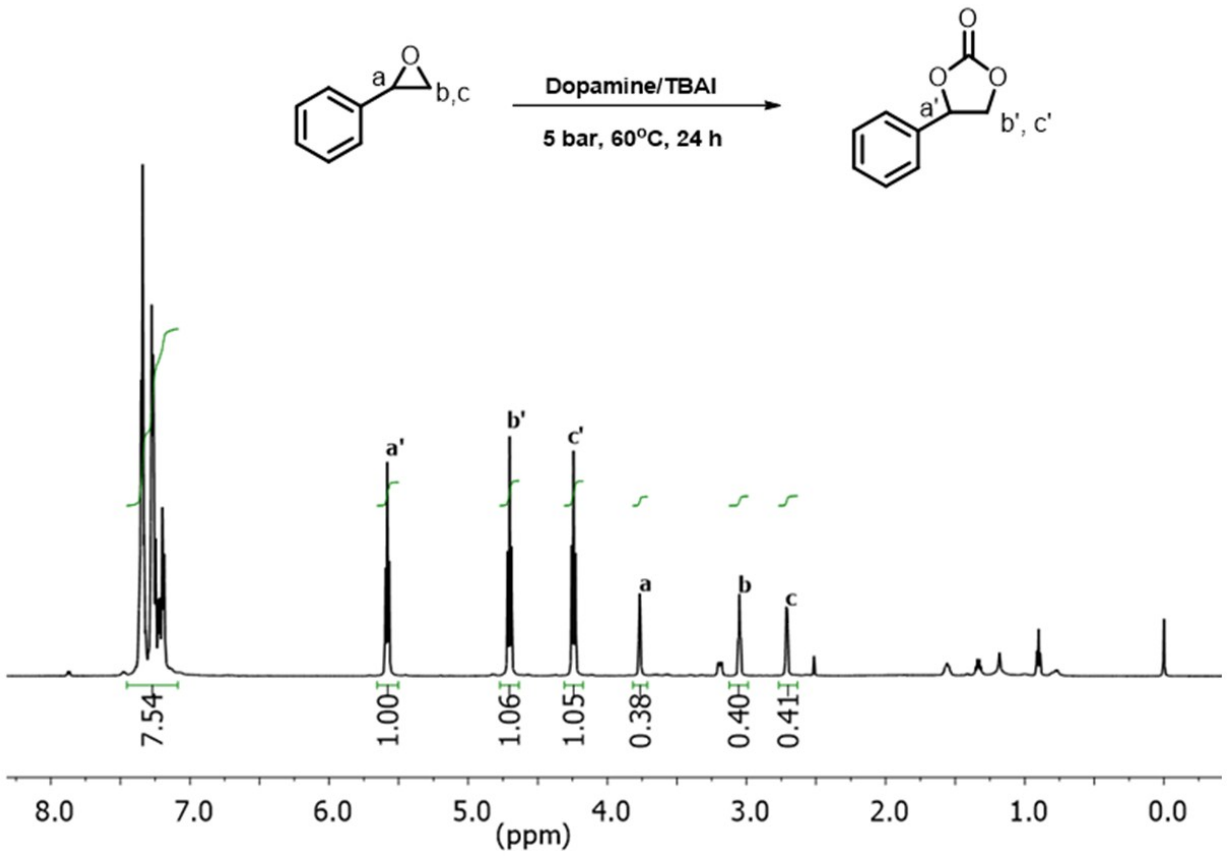

Figure S29. ^{1}H NMR spectrum of the product of the reaction between styrene oxide and CO_2 to afford styrene carbonate catalyzed by TBAI and dopamine (Table 2, Entry 11). Additional peaks in the spectrum arise from residual $CHCl_3$ in $CDCl_3$ (7.24 ppm), H_2O in $CDCl_3$ (1.6 ppm), TMS standard (0.0 ppm), and TBAI (3.26, 1.70, 1.35 and 0.9 ppm).

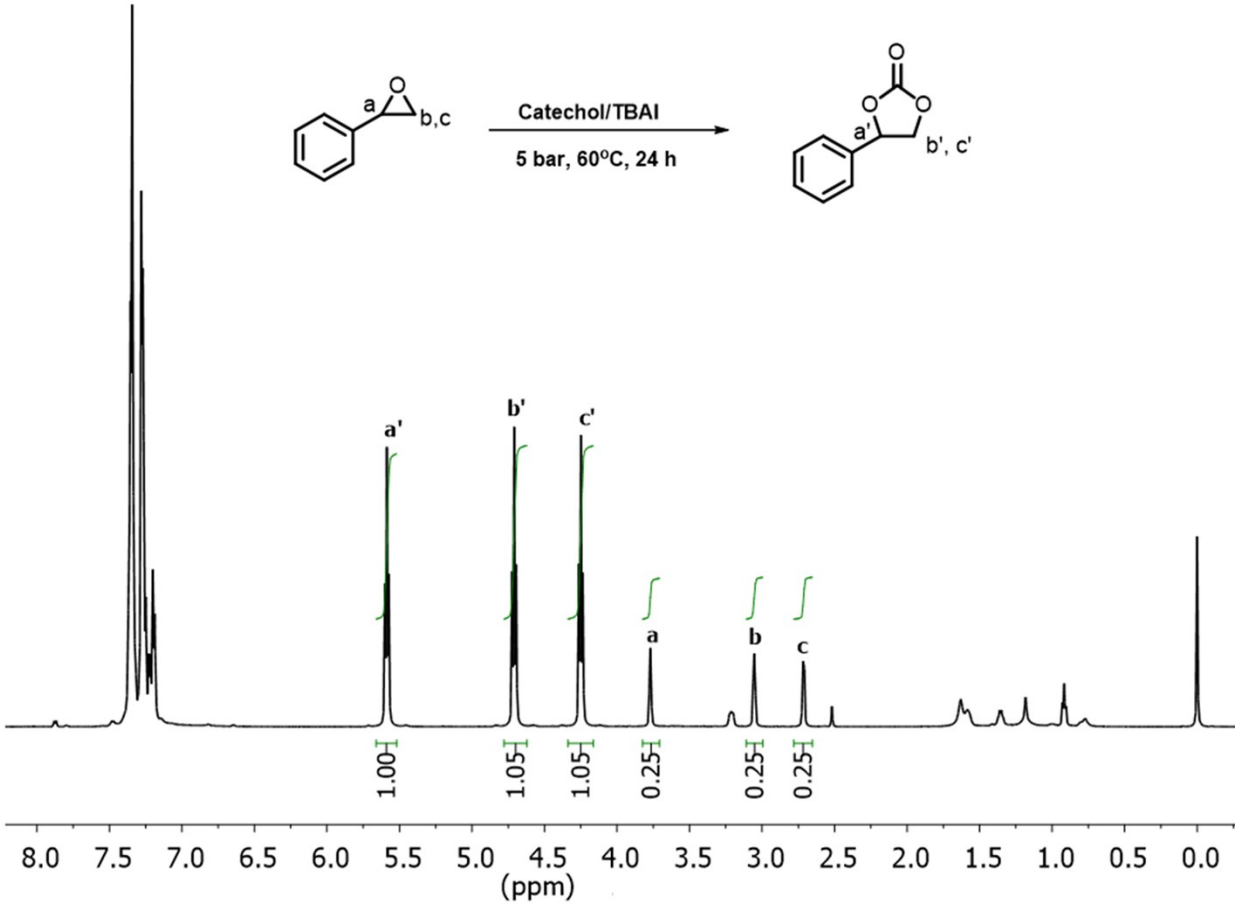

Figure S30. ^{1}H NMR spectrum of the product of the reaction between styrene oxide and CO_2 to afford styrene carbonate catalyzed by TBAI and catechol (Table 2, Entry 12). Additional peaks in the spectrum arise from residual $CHCl_3$ in $CDCl_3$ (7.24 ppm), H_2O in $CDCl_3$ (1.6 ppm), TMS standard (0.0 ppm), and TBAI (3.26, 1.70, 1.35 and 0.9 ppm).

Reference

1. Chu, D. H.; Vinoba, M.; Bhagiyalakshmi, M.; Hyun, B., II; Nam, S. C.; Yoon, Y.; Kim, S. H.; Jeong, S. K., CO2 mineralization into different polymorphs of CaCO3 using an aqueous-CO2 system. *RSC Advances* **2013,** *3*, 21722.